

Rochester Institute of Technology

RIT Digital Institutional Repository

Theses

7-2024

The Effect of Angiogenesis on Thermal Properties of In-Vivo Human Tissue

Shriya Musuku
sm5692@rit.edu

Follow this and additional works at: <https://repository.rit.edu/theses>

Recommended Citation

Musuku, Shriya, "The Effect of Angiogenesis on Thermal Properties of In-Vivo Human Tissue" (2024). Thesis. Rochester Institute of Technology. Accessed from

This Thesis is brought to you for free and open access by the RIT Libraries. For more information, please contact repository@rit.edu.

ROCHESTER INSTITUTE OF TECHNOLOGY
DEPARTMENT OF MECHANICAL ENGINEERING

**The Effect of Angiogenesis on Thermal Properties of In-Vivo
Human Tissue**

by

Shriya Musuku

A Thesis Submitted in Partial Fulfillment of the Requirements for the Degree of
Master of Science in Mechanical Engineering

Supervised by

Dr. Satish Kandlikar
Department of Mechanical Engineering
Kate Gleason College of Engineering
Rochester Institute of Technology
Rochester, NY
July 2024

KATE GLEASON COLLEGE OF ENGINEERING
The Effect of Angiogenesis on Thermal Properties of In-Vivo Human Tissue

By: Shriya Musuku

A Thesis Submitted in Partial Fulfillment of the Requirements for the Degree of Master of
Science in Mechanical Engineering

DEPARTMENT OF MECHANICAL ENGINEERING
KATE GLEASON COLLEGE OF ENGINEERING
ROCHESTER INSTITUTE OF TECHNOLOGY

Approved By:

Dr. Satish G. Kandlikar Date
Thesis Advisor
Department of Mechanical Engineering

Dr. Howard Tu Date
Thesis Committee Member
Department of Mechanical Engineering

Dr. Isaac Perez-Raya Date
Thesis Committee Member
Department of Mechanical Engineering

Dr. Sarilyn Ivancic Date
Department Representative
Department of Mechanical Engineering

ABSTRACT

Bioheat transfer is the study of heat transfer in biology. There are several sources of heat in biology including external ones such as surgical applications of heat, or internal ones like cancer tissue. Blood flow networks affect both types of processes and are often generated during disease phenomenon through a process called angiogenesis. This affects the properties of the tissue. Several attempts were made to model flow and heat transfer within various tissues through physical measurements or computer simulations. Both types of models used bioheat transfer models do not consider the geometry of vasculature at its most fundamental level.

The objectives of the research are to consider blood vessel diameter, length and flow direction to determine how each impacts the effective thermal conductivity in live tissues. This work used Computational Fluid Dynamics techniques and anatomical properties of blood vessels to create a parametric study of how non cardiac vasculature affects tissues. Validation was conducted using Gautherie's data on the effective thermal conductivity of the breast as a case study. The analysis was conducted in both 2D and 3D and extended to include implications of the heat source and multiple vessels on the thermal properties of the tissue.

ACKNOWLEDGMENTS

I have been working with the Thermal, Microfluidics and Fuel Cell Lab (TAMFL) under Dr. Kandlikar's guidance since joining as a student in the undergraduate independent research program. I have grown so much as an engineer and a person over the past five years of working with him. He encouraged me to take pride in my work and taught me to tell my story with confidence. I thank him for his mentorship.

I am also grateful for the mentors I have had in my years of working in the lab, including Dr. Alyssa Owens, my first PhD mentor, Dr. Maharshi Shukla, who introduced me to the pool boiling side of the lab, and Dr. Carlos Gutierrez for his continued mentorship and friendship. A huge thank you to Dr. Perez for teaching me Computational Fluid Dynamics and for accelerating my research writing to the next level. The past five years would not have been complete without my TAMFL lab mates and friends who helped me through the hardest parts of an engineering degree. They were the best I could ask for. I appreciate them for the jovial and supportive atmosphere they have created even while working.

This work is dedicated to my family – my mother, father, sister, and grandmother. A fair portion of life was challenging with illness, the passing of those we hold dear, and the tough process of immigrating to the US. I see the hard work we've put into coming out through it all. Thank you for the love and support that helped me become who I am today.

TABLE OF CONTENTS

ABSTRACT.....	2
ACKNOWLEDGMENTS	3
LIST OF FIGURES	6
LIST OF TABLES	8
NONMENCLATURE.....	9
1.0 INTRODUCTION	10
2.0 THE RESEARCH QUESTION	13
3.0 LITERATURE REVIEW	14
3.1 Introduction to Bioheat Transfer and Biofluid Mechanics	14
3.2 The Biology of Cancer: Study of a Common Phenomenon in Human Tissue	16
3.2.1 Understanding Normal and Cancerous Human Physiology	16
3.2.2 Key Biological Changes in the Tissue During Cancer Formation.....	16
3.2.3 Effect of Biological Changes Caused by Cancer on Tissue Level Processes.....	17
3.3 Principles of Fluid Dynamics in Human Tissue	19
3.3.1 Biofluid Mechanisms that Affect Fluid Flow Behavior	19
3.4 Modeling Human Vasculature	21
3.4.1 Common Assumptions.....	21
3.4.2 A Breakdown of Cell Based Vascular Modeling Methods.....	22
3.4.3 Computational Flow Modeling Methods.....	24
3.4.4: Advanced Tools for Modeling and Their Pitfalls	25
3.5 Bioheat Transfer Applications in Human Tissue.....	28
3.5.1 Forms of Heat Transfer in Humans	28
3.5.2 Key Parameters Used in Heat Transfer in Biological Tissue	29
3.5.3: One Focused Application – Breast Cancer and its Thermal Significance	29

3.6 Bioheat Transfer Models Used in Computation	32
3.6.1 Pennes' Bioheat Transfer Equation	32
3.6.2 Other Bioheat Transfer Models	33
4.0 OBJECTIVES OF THE PROPOSED WORK	36
5.0 METHODS	37
5.1 Theoretical Background and Key Assumptions	37
5.2 Computational Domain and Boundary Conditions.....	39
5.3 Computational Mesh.....	41
5.4 Governing Equations	43
5.5 Ansys Customization	45
6.0 RESULTS AND DISCUSSION.....	46
6.1 Mesh Sensitivity Analysis Outcomes	46
6.2 Results of Verification and Validation	47
6.2 Outcomes of the 2D Parametric Simulations.....	59
6.3 Outcomes of the 3D Parametric Simulations.....	61
6.4 The Impact of Multivessel Flow on Effective Thermal Conductivity	63
6.5 Use of Effective Thermal Conductivity as a Substitute to Vasculature.....	64
7.0 CONCLUSION.....	66
8.0 LIMITATIONS AND FUTURE WORK	68
9.0 SOCIETAL CONTEXT.....	69
10.0 REFERENCES	70

LIST OF FIGURES

Figure 1: Macrocirculation issues to consider in biofluid mechanics and heat transfer within tissues, reproduced from Rubenstein [7]	11
Figure 2: Microcirculation issues to consider in biofluid mechanics and heat transfer within tissues, reproduced from Rubenstein [7]	11
Figure 3: An Example Process of Cancer Development: Energy Flow in Breast Cancer as Derived from the Study of Biochemical Changes Involved [17] [22].....	17
Figure 4: Vessel Wall and Blood Transport Interactions in Tumor Blood Vessels, reproduced from Reiger et.al [24].....	18
Figure 5: Tumor Induced Angiogenesis Showing the Resulting Increase of Cell Structures and Biochemical Interactions in Tumor Formation, reproduced from Koumoutsakos et. al [25].....	18
Figure 6: Blood Flow Derived Forces that Affect Blood Circulation, reproduced from Campinho et. al [32]	20
Figure 7: Example Schematic that Determines How Vessels Branch and Elongate. Here, L is Length, and S is Cross Section of the Vessels, reproduced from Mada and Tokhiro [38].....	23
Figure 8: Framework of the CFD Procedure for Modeling Blood Flow, Vasculature, and Vascular Diseases Through Medical Imaging, reproduced from Kamada et. al [44].....	25
Figure 9: Computational Modeling Methods that Account for Cell, Tissue, and Organ Level Interactions, reproduced from Metzcar et. al [53]	27
Figure 10: Anatomy of a Healthy Breast, reproduced from Camilleri et.al. [57].....	30
Figure 11: Infrared Imaging and IRI Numerical Engine Computation of the Cancer Location using Modeling Methods, reproduced from Gutierrez [61].....	31
Figure 12: Overview of the 2D tissue composite, with parametrized variables labeled and a resistance diagram along the direction of heat flow	40
Figure 13: Overview of the 3D tissue composite, with parametrized variables labeled.....	41
Figure 14: Picture of Fine Computational Mesh.....	42
Figure 15: Picture of Fine Computational Mesh, with inflation layers and smaller fluid body sizing displayed.....	43
Figure 16: Heat Flow Schematic for 2D geometries, visualized by default as parallel plate in by Ansys Fluent computation	51
Figure 17: Visualization of Effective Thermal Conductivity in the Human Body.....	51

Figure 18: Pressure Drop within the Blood Vessel Embedded in the Computational Geometry for the Models comparing Newtonian and Non-Newtonian Flow	54
Figure 19: Temperature Contours of the Computational Domains Comparing Newtonian and Non-Newtonian Flow Models.....	54
Figure 20: Temperature Contour the Blood Vessel Embedded in the Computational Domain, Comparing Newtonian and Non-Newtonian Flow Models	55
Figure 21: Impact of Top Wall Temperature on Effective Thermal Conductivity of fatty tissue and the Use Cases of the Wall Temperatures	56
Figure 22: Measured temperatures and effective thermal conductivity, a) comparing a healthy and cancerous breast using measurements b)depicting cancer progression over time and c)showing change with treatment from Gautherie and recreated by Gutierrez [61] [56].....	58
Figure 23: Diameter versus Effective Thermal Conductivity 2D Parametric Study	59
Figure 24: Velocity versus Effective Thermal Conductivity 2D Parametric Study	60
Figure 25: Length versus Effective Thermal Conductivity 2D Parametric Study	61
Figure 26: Diameter versus Effective Thermal Conductivity 3D Parametric Study	62
Figure 27: Velocity versus Effective Thermal Conductivity 3D Parametric Study	63
Figure 28: Length versus Effective Thermal Conductivity 3D Parametric Study.....	63
Figure 29: Effective Thermal Conductivity and contour comparison of multivessel flow configurations	64
Figure 30: Temperature Contours of Solid Tissue without Vasculature and Tissue with an Embedded Vessel.....	65

LIST OF TABLES

Table 1: Mathematical Equations Historically used in Breast Cancer Thermal Models, reproduced from Mashekova et. al [62]	32
Table 2: Anatomical dimensions and flow conditions of the parametrized vessels [9] [16] [58]	38
Table 3: Material Properties of Blood and Fat Tissue Used in Simulation [57] [58] [59] [60]....	39
Table 4: Computational Mesh Characteristics for the 4 Mesh Types in 2D Simulation	42
Table 5: Computational Mesh Characteristics for the 4 Mesh Types in 3D Simulation	43
Table 6: Mesh Sensitivity Analysis Results for the 4 Mesh Types in 2D Simulation.....	46
Table 7: Mesh Sensitivity Analysis Results for the 4 Mesh Types in 3D Simulation.....	47
Table 8: Pressure Drop Validation for 2D Geometry	48
Table 9: Pressure Drop Validation for 3D Geometry	49
Table 10: Temperature Drop Validation for 3D Geometry	53

NONMENCLATURE

Angiogenesis	=	Development of new blood vessels in tissue
Bioheat transfer	=	The study of heat transfer in biological materials
Biofluid mechanics	=	The study of fluid dynamics in biological materials
c_p	=	Specific heat
CFD	=	Computational Fluid Dynamics
<i>EC</i>	=	Endothelial Cells
<i>In-Vivo</i>	=	In live tissue
<i>In-Vitro</i>	=	In extracted tissue, literally “in glass”
k	=	thermal conductivity
k_{eff}	=	Effective thermal conductivity
ρ	=	Density
μ	=	Viscosity
UDF	=	User Defined Function
VEGF	=	Vascular Endothelial Growth Factors
w	=	perfusion rate
X_{ent}	=	Entrance effects

1.0 INTRODUCTION

Heat transfer is studied in the human body in the context of heat exposure, circulation, biochemical reactions, and the treatment and diagnosis of malignant conditions such as cancer or cardiac abnormalities. The field that studies thermal transport through tissue is called bioheat transfer. The fundamental modes of bioheat transfer are the same as that in traditional mechanical engineering: conduction, convection, and radiation. Any heat generation process considered in this field is typically metabolic in nature. The key parameters needed to study heat transfer in tissues are the thermal conductivity, specific heat, tissue perfusion, and the properties of thermal tissue (density and viscosity) [1] [2].

Thermal conductivity, k , is the “steady state ability of an object to conduct heat when subject to a temperature gradient on its surface”. The specific heat, c , is “the amount of thermal energy stored in a material at a certain temperature”. Tissue perfusion is characterized as the volume of blood moving per unit of time in the tissue. Perfusion effects are often lumped into a singular perfusion rate term, w , defined as the mass flow rate of blood per volume of tissue [1]. The core body temperature of humans is 310 K (36 °C to 37 °C). Blood perfusion creates additional heat transfer proven by measurements [3].

Bioheat transfer has several applications. Heat signatures were found in both breast cancer and basal cell skin cancer, which have a unique temperature signature that can be detected using infrared thermography. Thermal imaging in skin cancer is conducted with steady state or dynamic imaging. Cold stimuli can be applied to disturb the existing equilibrium and enhance the detection of any abnormalities. Modeling techniques have been created using bioheat transfer theory to predict the relationships between thermal scans and the location of cancer. Newer computational tools are being used to improve the clinical detection and treatment methods of physiologies that have bioheat transfer signatures [4].

One very influential study on breast cancer was conducted by Gautherie in the 1980s. His research was the first and only significant in-vivo study of the “Thermopathology” of breast cancer. The heat distribution profile of several patients was measured, and properties such as thermal conductivity and metabolic heat generation were graphed. Probes and thermal camera techniques were also used in these early bioheat transfer experiments. These signatures were primarily caused by the generation of vasculature in the cancerous soft tissue [5] [6].

Blood flow creates a significant temperature difference due to the added convection that it brings. Angiogenesis, or the development of blood vessels, occurs in breast cancer and increases perfusion. This phenomenon was also observed within kidney, retinal, and pancreatic cancers, lacerations, and in embryos. The studies conducted regarding the development of vasculature within the human body led to the development of a subject called biofluid mechanics. This subject studies fluid mechanics in biological systems and accounts for differences in viscosities, other fluid structure interactions including macrocirculation (for instance, arterial versus venous flows in Fig. 1) and microcirculation issues (interstitial fluid flow, thermal interactions, etc. in Fig. 2).

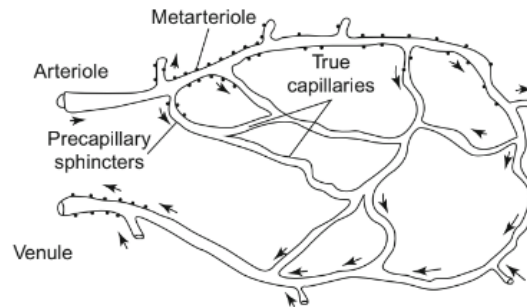


Figure 1: Macrocirculation issues to consider in biofluid mechanics and heat transfer within tissues, reproduced from Rubenstein [7]

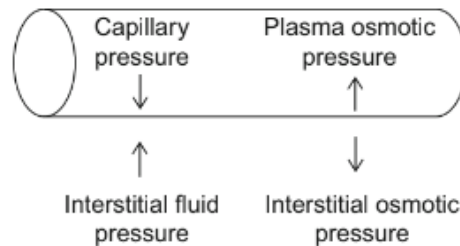


Figure 2: Microcirculation issues to consider in biofluid mechanics and heat transfer within tissues, reproduced from Rubenstein [7]

Griffioen has combined the study of heat transfer and biofluid mechanics and found that blood flow and vessel development have a significant impact on tissue properties, including within angiogenic cancers [8]. In general, heat transfer is affected by the following factors: vessel geometry, rate of blood flow, and the amount of perfusion in each tissue. While the blood leaving the aorta does not exchange energy with the tissue, the process of thermal equilibration

really begins in the primary arteries and completes by the time it reaches the end capillaries [3]. The thermally significant vessels that are smaller than the large artery branches cause such temperature changes are the focus of this study.

One function of blood circulation is to maintain the body's energy balance. The basic model of bioheat transfer uses standard thermal diffusion equation and applies it to biological processes. The effects of conduction through the tissue, blood perfusion, and metabolic heat transfer are all added up to contribute to the total heat transfer. This model evolved into the Pennes's bioheat transfer equation that has good agreement with the measured values of heat transfer in tissues. Yet, this model fails to look at blood flow direction, anatomical measurements, and falsely assumes that arterial blood flow does not change temperature as it reaches the capillary bed. The model also simplifies metabolic heating, perfusion rate, and thermal conductivity to a constant value despite these values having cross interactions and complicated responses. Subsequent models attempted at mitigating these limitations through their own approaches at varying degrees of involvement in measuring vessel geometries and flow conditions [2] [9].

The effective thermal conductivity model was proposed by Weinbaum and Jiji to consider the local perfusion rate and vascular figure. It used k_{eff} , a composite conductivity parameter considering the tissue and blood flow as one system with a unique conductivity based on the composition and organization of vasculature. The model is very simple and considers the cross sectional geometry, advection, inherent tissue and blood conductivity, and the radius of the artery to generate an effective conductivity value. The work is a great starting point in determining how the dominant vessels in a tissue cross section impact conductivity but has significant limitations. The research states that it is best suited for models near the skin surface [10]. It also is inaccurate for results above 200 μm , and focuses on countercurrent exchange between arteries and veins rather than the impact of individual geometry [2].

With these limitations in mind, there is a need to determine which biological factors impact effective thermal conductivity in a tissue with angiogenesis. Vessel diameter, length, flow velocity, and the number of vessels will be considered in relation to the conductivity of a tissue system. Fatty breast tissue will be used to confirm the results with Gautherie's work, as a case study of the impact of vasculature. This research will improve the in-vivo models and the understanding of heat transfer in human tissues.

2.0 THE RESEARCH QUESTION

Bioheat transfer impacts tissue systems through internal biochemical processes, thermoregulation due to external changes, and through heat transfer driven processes such as surgeries and cancer [11]. Heat transfer research influences tissues and treatment methods, and one such case happens when there is a high concentration of existing or developing blood vessels. The process of angiogenesis, where new vasculature is generated in existing tissue, is a common pathway for heat transfer in cancers [5].

Several models have been developed to depict the heat transfer within tissues. One of these is the Penne's bioheat model, and another is the effective thermal conductivity model that describes the total thermal conductivity of tissue system as a composite of all the internal heat transfer processes. All models simplify tissue thermal conductivity and use generalized measurements of thermal conductivity in their approach [2]. These assumptions have not been tested for the validity of implications they inherently include. In particular, the perfusion rate, a key parameter, is a measurement of density of the blood vessels. Yet, there is little theory on how the geometry of blood vessels and the flow properties of the capillaries, arterioles, and arteries impacts bioheat transfer.

Further research into this topic can improve the understanding of the vasculature impacting bioheat transfer and contribute to the fundamental theory. There are several relevant applications including cryosurgery, ablation, cancer development, and thermal scanning. There are two research questions for this study:

1. How does vascular geometry impact the effective thermal conductivity of a tissue system with blood flow?
2. Can a simplified model be generated using effective conductivity that closely matches the vasculature models?

3.0 LITERATURE REVIEW

The following sections provide an overview of the important models used in bioheat transfer, and their implementation via math, experimentation, and simulation. A discussion of the human body in correlation to health and disease is included to enhance the understanding of bioheat transfer. Cancer is highlighted as a particular example of a complex phenomenon that affects human tissue and has significant societal impact. The applications of bioheat transfer can be extended further to procedures such as ablation, cryosurgery, and radiation treatments in several types of tissues.

The research conducted in this thesis focuses on an average fatty tissue, commonly found in the female breast. This type of tissue was selected due to the readily available of research, and significant experimental data available due to Gautherie's research, which is also highlighted.

3.1 Introduction to Bioheat Transfer and Biofluid Mechanics

Heat transfer occurs in cells, tissues, and organs and impacts the human body at every level. Organ level studies are conducted using computational models that are often coupled with patient data collected through various scanning modalities including MRI, Angiograms, etc. Individual tissue properties and calorimetry applications are included in the study of heat transfer and are the basis of generic thermal models that study perfused tissues. The study of live ("in vivo") tissue is affected by the generation of blood vessels. While there are smaller effects such as interstitial fluid exchange in blood vessels, their primary function is the thermoregulation of the human body as it undergoes metabolic changes [1].

The key parameters that are used in heat transfer in biological tissue include thermal conductivity, specific heat, and perfusion rate. Other parameters to be considered include vessel size and density, direction of fluid flow, viscosity of blood, etc. The fluids in the blood vessels undergo elemental stress and pressure in all six directions as they move through the system. The governing laws used in biofluid mechanics are the same as those in fundamental mechanical engineering. These include the Navier Stokes equation, conservation of mass, conservation of momentum, and the conservation of energy. Fluid is viewed as a continuum in these models, following the laws kinematics while still having bulk properties of viscosity and cohesion involved. These systems combine microcirculation, on the cardiac level, with microcirculation that occurs due to capillary interactions to the complex dynamics involved in human tissue [7].

The effect of porous media and cell adhesion may be of impact in heat transfer on a cellular level but is often neglected in tissues due to the exchange being insignificant in mass. Typically, “mass transport is largely restricted to the smallest blood vessels, capillaries, arterioles, and venules”[12]. In contrast, heat transport occurs in thermally significant blood vessels that are larger than 80 micrometers but are not large supply vessels. These blood vessels are numerous and tend to be densely packed [12].

The primary thermal interaction in perfused tissue is the heat conduction through blood vessels. Additionally, advection and bulk fluid properties are often averaged over the larger matrix. Blood volume is considered more variant and relevant when assessing smaller tissues. The extracellular matrix of the tissue is very similar in thermal conductivity of the vessels walls, allowing for the resistance and contact regions to be considered negligible [12]. The blood vessels in this smaller region are considered to have equilibrated as this process happens very quickly after the supply vessel branches out into a densely packed smaller network. The surrounding tissue contributes significantly to the equilibrium due to the increased surface area. Heat transfer increases directly with a ratio of the depth and radius of the vessel [13] [14].

Microcirculatory heat transfer uses the conservation of energy as its governing equation, as reproduced from Rubenstein et. al [7].

$$\dot{E}_{fluid} = \dot{m}c_p T_m = \int_0^A \rho c_p T(r)u(r) \text{ (Eqn. 1)}$$

Here, E signifies energy, A is the cross sectional area, m is the mass flow, c_p is the specific heat, and u is the radial coordinate of the system. This energy balance can be used to solve for the heat transfer rate, as reproduced from Rubenstein et. al [7].

$$\dot{Q} = \dot{q}_s A_s = \dot{m}c_p(T_o - T_i) \text{ (Eqn. 2)}$$

Here Q is the heat transfer rate, and q is the surface heat flux of the analyzed cross section. This formula can be used to calculate temperature drop within a pipe using the principles of conduction, convection or radiation. These two equations remain the basis of bioheat transfer where there is circulation involved. Multiple parameters are combined to account for this full energy balance and to simulate heat fluxes caused by increased energy generation. Additional theory of medical phenomena is discussed prior to introducing detailed bioheat transfer models.

3.2 The Biology of Cancer: Study of a Common Phenomenon in Human Tissue

3.2.1 Understanding Normal and Cancerous Human Physiology

Normal human anatomy and physiology starts at the cell level (for example, endothelial cells). There are several types of cells that when put together become a tissue (for example, an organ lining). A few types of tissues when combined form and a full organ (for example, the stomach). A few organs together form an organ system (for example, the digestive system). The human body is a combination of many such organ systems which function in harmony and are, in theory, self-regulating to function with proper anatomical and physiological properties. The body responds to several external phenomena and maintains equilibrium. Yet, there are conditions in which the human body is unable to self-correct, due to which the field of medicine arises. While there are several situations in which human tissue requires treatment, cancer is one such complex condition whose study benefits humanity and has several cross applications [15] [16].

Cancer is a mass of cells that grows uncontrollably due to trigger conditions such as cellular mutations caused by spontaneous radiation, viral, genetic, or other environmental conditions. The cascade of events leads to the group of cells becoming invasive and taking over normal bodily processes and affecting or even taking over the functioning of several processes within the vascular, lymphatic, immune and organ systems [17] [18].

3.2.2 Key Biological Changes in the Tissue During Cancer Formation

Tumor growth is based on complex interactions that are further triggered by unique conditions such as low oxygen and low glucose levels caused by the cancer. The in-vivo cancer metabolism first starts with increased carbon consumption in tumor cells. The cells are highly glycolytic [17]. They consume a lot of energy, primarily in the form of glucose, which is a carbon compound. With such growth comes an increase in hypoxia which leads to a metabolic pattern of seeking more energy and oxygen, often in the form of blood vessel generation in the area. This process of blood vessel generation is called angiogenesis and is a significant discovery due to the impact it has on multiple organ systems [19]. It affects lymph nodes in the area, the chances metastasis, and primarily has a positive correlation with certain types of cancer (breast, retinal, and kidney cancer are common examples) [20] [21].

Cancer also leads to increased fluid transfer with interstitial fluid, several types of growth factors, and an overall increased pressure in the area due to uncontrollably growing cells. Solid

cancers develop into lumps, and other cancers such as leukemia (blood cancer) flow within the body [7]. The biochemical reactions within the system lead to a self-perpetuating cycle of processes that divert the regional resources away from normal bodily function and instead escalate cancer growth until it becomes unsustainable. Only tissue systems and solid cancers are applicable for the scope of this thesis.

The biochemical changes start with finding an energy source such as fat tissue. The breakdown of this tissue fuels a cancer through processes such as angiogenesis which then brings more energy to the area through blood flow which aids cell respiration. Likewise, the risk of cancer metastasis increases over time [17]. One such example process is detailed for the energy flow through the chemical processes shown in Fig. 3 below.

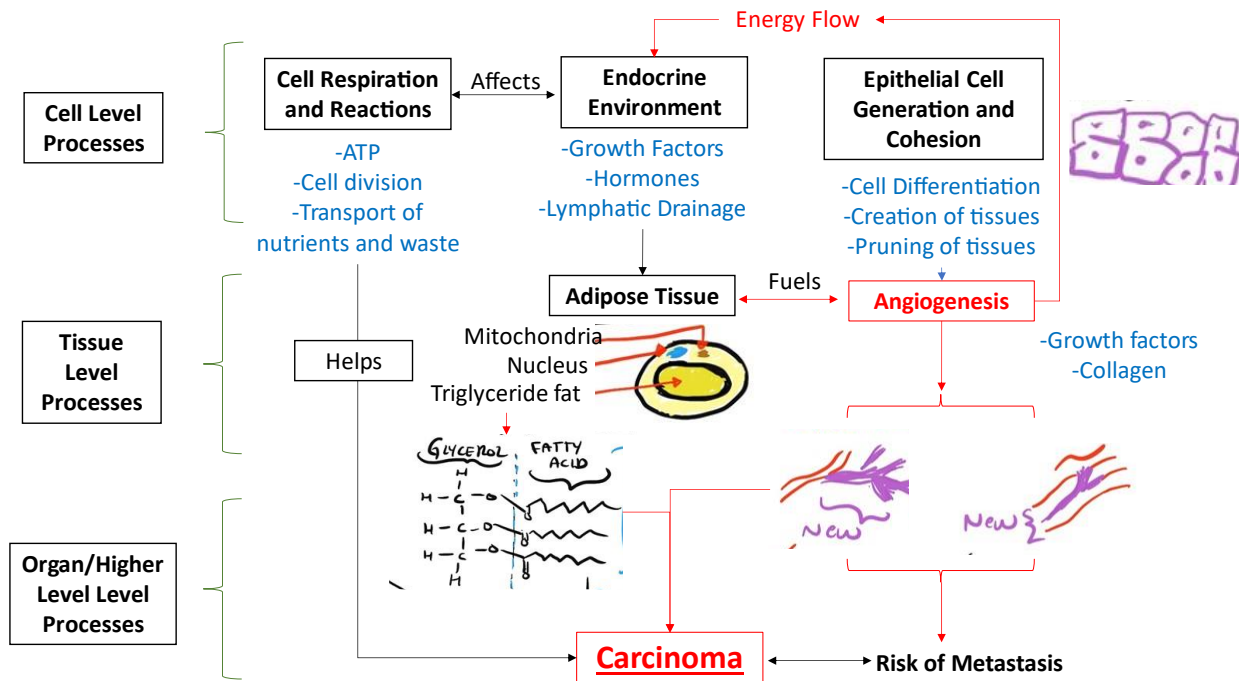


Figure 3: An Example Process of Cancer Development: Energy Flow in Breast Cancer as Derived from the Study of Biochemical Changes Involved [17] [22]

3.2.3 Effect of Biological Changes Caused by Cancer on Tissue Level Processes

The biochemical processes described in the previous sections have effects on the matrix of cells that surround them. Particularly, solid cancers are noted to increase the shear stress in cells as the mass develops. Angiogenesis causes blood vessel formation and is a common process in some cancers. Their new blood vessels are so haphazard that they are often called “torturous blood

vessels” which don’t have the well-developed matrix or structure of normal physiology [23]. With the increase in shear stress and blood vessel formation, there is an increase in interstitial pressure as new cells and chemicals flood the area. The cells become packed in the area, start vying for nutrition and have poor drainage that they also cause swelling of the lymph nodes and change organ function. An illustration of the key transport phenomenon and cellular interactions are shown in Fig. 4 and 5.

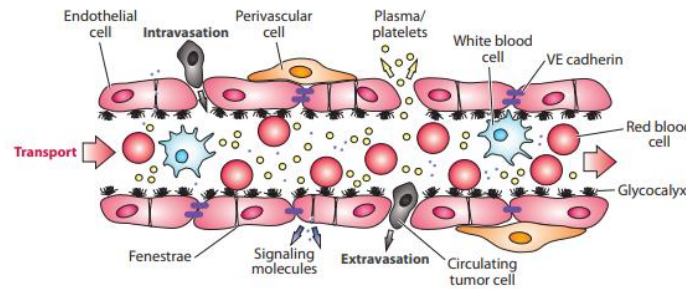


Figure 4: Vessel Wall and Blood Transport Interactions in Tumor Blood Vessels, reproduced from Reiger et.al [24]

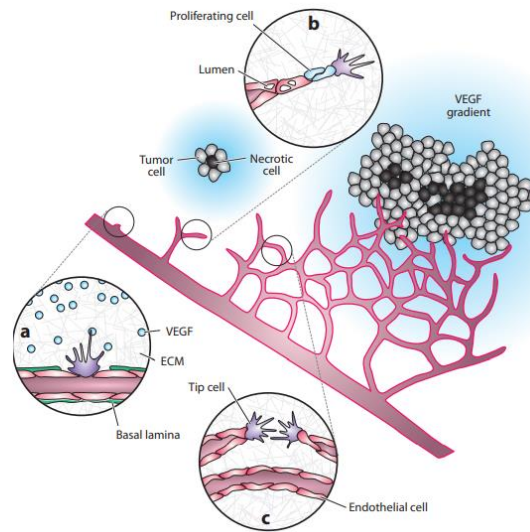


Figure 5: Tumor Induced Angiogenesis Showing the Resulting Increase of Cell Structures and Biochemical Interactions in Tumor Formation, reproduced from Koumoutsakos et. al [25]

Fig. 5 shows the blood vessel formation inconsistency and depicts the leaky vessels that form during cancer. They still transport blood cells, but the outside endothelial cell matrix doesn’t

have structural integrity and allows for small chemicals to enter and leave the cell. Meanwhile, circulating tumor cells line the blood vessel and take energy from the angiogenesis such that the rest of the region doesn't receive the energy it needs. To counter this, angiogenesis continues [25].

A fast way of generating new blood vessels is to break down an existing vessel and use growth factors to create a new endothelial cell matrix that protrudes from the original matrix. The new cells that grow from the growth factors to make the new blood vessels are called the proliferating cells. The tumor sits right at the location of angiogenesis and grows [25]. The process of necrosis is depicted in Fig. 5, which happens when the tumor grows too big, and the inner portion dies out as it can't receive energy and oxygen from the blood vessels surrounding it.

The tumor then grows fast and the biochemical interactions, new blood flow, and growth create a heat profile in the case of breast cancer. The physical changes mentioned were observed through several thermal scans that differentiated the source of the heat from the rest of the body.

Angiogenesis and fluid transport became a huge point of research in the 2010s [26] [27]. Modulation of the glycemc elements and oxygen content was shown to be a key regulator of angiogenesis. An increase in hypoxia and a decrease in glucose were shown to spark tumor growth and blood vessel formation. Then, when combined they were shown to have a significant impact on rapid tumor growth. The condition when there is hypoxia in a low glucose cancerous environment was known to be the "angiogenic trigger" where the blood vessel development increases rapidly [28] [29] [30].

3.3 Principles of Fluid Dynamics in Human Tissue

3.3.1 Biofluid Mechanisms that Affect Fluid Flow Behavior

With the growth of blood vessels in tissue, the subject of fluid dynamics in tissue cross sections came into scrutiny. The subject, now called biofluid mechanics, explores the biological elements as they relate to the physical effects of fluid flow throughout the body. First, the development of blood vessels happens through the angiogenic triggers described. Angiogenesis happens in healthy bodies during pregnancy and growth, and in unhealthy tissues during cases that include the development of masses, lumps, or cancers.

The endothelial cells (ECs) in angiogenesis work by separating the interior of the blood vessels from the surrounding tissues. They create a tight barrier that maintains a function of protecting the blood vessels while still having the ability to be formed and remodeled over time. Blood circulation generates forces that act on the ECs to drive flow changes to areas that need blood supply, allow for regular network pruning, and to transition new and old cells out of circulation. The cell type is called the endothelium squamous cell monolayer as there are several different endothelial cell types throughout the body. They form the network of tubes and primarily develop during embryogenesis. The key forces that act on a blood vessel are the circumferential stresses, shear stresses and axial stresses as given in Fig. 6. The presence of fluid flow forces has a positive impact on the development of cancer [24] [31].

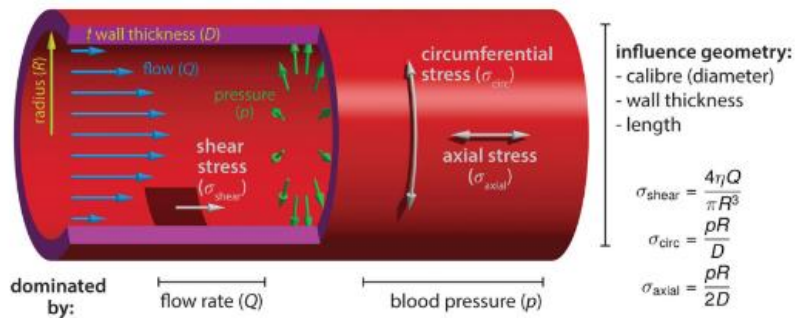


Figure 6: Blood Flow Derived Forces that Affect Blood Circulation, reproduced from Campinho et. al [32]

Endothelial cell behaviors affect four major processes in the circulatory system: 1) regulation, 2) sprout formation and elongation 3) pruning and maintenance and 4) valve formation and maintenance. Angiogenesis in disease happens through the first two processes and is typically formed with little regulation and pruning. The circulation diagram also studied the size of vessels and found that vessel sizes adjust themselves to the flow. This happens through endothelial cell sensitivity and the bio tensegrity in the tissue. That is, the cells have a dynamic feedback loop that involves sensing shear forces on individual cells and their collective tissues, due to which adjustments are made to accommodate blood flow stress patterns to the needs of the body. Additionally, it was found that the arteriolar tissue is formed by a two-layer fiber reinforced hyperplastic material. This model uses pressure within the vessels to determine the thickness of

the walls, showing that hemodynamic features such as the viscoelasticity of blood affect the thickness of vessel walls creating a complete feedback loop for biofluid mechanics [33].

3.4 Modeling Human Vasculature

The key factors involved in modeling tissue cross sections are the biological/biochemical processes in tissue, fluid flow, and heat transfer. While each element has been discussed individually, some research has been conducted on vascularized tissue systems in the presence of all three elements. The primary assumptions, modeling methods, and computational tools used in the models are discussed in this section.

3.4.1 Common Assumptions

Vasculature has been modeled to understand the internal processes involved in normal and abnormal tissues. The elements that have been considered in this effort include cell signaling and molecular aspects of vessel formation, and then the cell-based models that allow for proliferation and maturation of the formed vessel structures in cancer tissue. Lower-level models use molecular structures to understand cells and cell structures to depict tissues. The most helpful simulations tie both elements into whole organ and tissue models that the full picture. Based on the patterns, tissue models had the following assumptions that will also be used in the thesis.

The first assumption is that the necessary growth factors (typically called VEGFs) and their receptors form the pathways for tissue development that are every present [28]. That is, these growth factors and biological pathways required to support tissue existence and development are assumed to be stabilizers within the system. This is particularly important as the models in this proposal focus on live tissue.

The second assumption is that there is a hybrid discrete continuum within tissues that have tumor induced angiogenesis. That is, the biochemical elements within the tissue develop progressively, but have certain triggers that speed up angiogenesis or tumor growth. Additionally, blood flow and forces change the vascular networks dynamically, and they adapt to their surroundings [34] [35]. This is an important observation that changes the models that involve vascular growth. This thesis takes different scenarios and determines the effect of vasculature on heat transfer within tissue but does not focus on modeling the dynamic changes of the vasculature itself. Therefore, the scenarios considered will simply take various parameters in vascular growth and assume that

they are in steady state equilibrium, rather than also attempting to model the vasculature in dynamic forms.

The third assumption made is to use blood as a Newtonian fluid to simplify calculations. Blood is Non-Newtonian. The variable viscosity is modeled using one of two options, the Casson or Power Law equations given below, and reproduced from Husain et. al [36].

The Casson model was defined as:

$$\mu = \frac{[\sqrt{\tau_y} + \sqrt{\eta|\dot{\gamma}|}]^2}{|\dot{\gamma}|} \text{ where } \eta = \eta_0(1 - H)^{2.5}, \tau_y = 0.1(0.625H)^3$$

with $\eta_0 = 0.0012 \text{ Pa} - \text{s}$ and $H = 0.37$ (Eqn. 3)

The Power Law model is defined via the equation:

$$\mu = \mu_0(\dot{\gamma})^{n-1} \text{ where } \mu_0 = 0.01467 \text{ and } n = 0.7755 \text{ (Eqn. 4)}$$

In these equations, μ is viscosity, τ is shear, and η and H are constants used in modeling.

Lastly, blood perfusion and interstitial fluid effects have been a point of contention in several fluid flow models. While both have been found to be important, several models take tissue cross sections outside of the human body where they don't apply [37]. This work considers the interstitial effects insignificant as they are very small scale and don't impact heat transfer as much as the blood flow.

3.4.2 A Breakdown of Cell Based Vascular Modeling Methods

The cellular and vascular networks were modeled through a pattern formation analysis in which elongation and bifurcation were considered the two key parameters of a typical vascular geometry. Vasculature was generated using a radial space filling model within the paper to show the effects of complex networks. The model also uses the assumption that tip cell growth is a key contributor to the development of vasculature and thoroughly considers the biological effects and growth factors acting on tissues. Therefore, the key takeaway for this paper is the detail on branching, and the formulas they provide on the mechanism with which this happens. An example of the process used is given in the Fig. 7 below [38]. These models are not entirely

applicable for this thesis as they aren't based on live tissue. Still, the paper highlights the geometries that should be considered when modeling more advanced tissue systems.

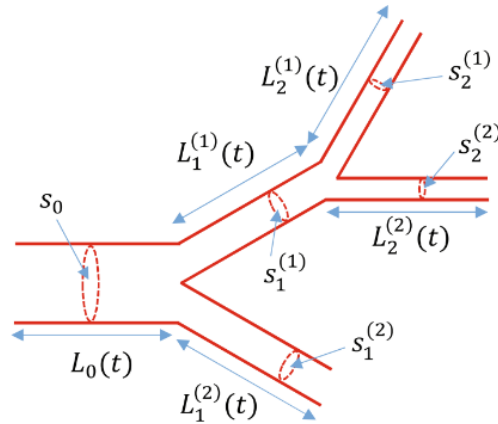


Figure 7: Example Schematic that Determines How Vessels Branch and Elongate. Here, L is Length, and S is Cross Section of the Vessels, reproduced from Mada and Tokhiro [38]

Several vascular models used space filling and differential equation models to optimize bifurcation. While the previous paper used elongation and bifurcation as the key parameter, other models also used blood flow distribution and vascular completion as parameters to consider. They may be helpful in progressing work in abnormal physiology where branching isn't the only criterion and haphazard angiogenesis takes place more often than space filling methods. This thesis only considers single vessel flow to understand its relationship to effective thermal conductivity, but this research can be an extended analysis of flow distribution in tissues in future work.

Lastly, the models found that shear stress and flow characteristics are negligible in 3D vascular models where the patient specific framework focuses on the structure rather than the growth pathways of the vasculature. This marked difference between angiogenic tissue and established tissue makes it important to consider the application of the vascular models and consider the assumptions carefully. [39].

The primary assumptions used in flow modeling include the circular tube assumption, steady state flow, ignorance of vessel wall thermal resistance, and interstitial flow in tissue level simulations. The tissue is considered non porous, and changes in perfusion with water and fat are often ignored impact of pulsative flow is also ignored in non-cardiac tissues [12].

3.4.3 Computational Flow Modeling Methods

Several fluid flow modeling efforts were conducted from the study of biofluid mechanics, studying cardiac function, vascular systems, and even utilizing biofluid principles in heat transfer applications. One such model is a multiscale flow model for blood regulation in a realistic vascular system. This model uses 1D vascular structure and assesses the porosity of the media and fluid exchange between arterial and venous capillary beds [23]. While it is an excellent method of understanding interstitial fluid flow, it does not reflect the 3D nature of tissue and provides only a partial understanding of the vessel structures. The model is applicable to this study because it can be extended into a spatial problem in multiple dimensions based on its simplification of the arteries, veins, and the capillary bed in the middle. It also provides insight into situations such as occlusion, which can help assess flow in improper vessels. Yet, it doesn't consider flow direction of the veins and arteries as it simply focuses on interstitial regions and the exchange of matter between the blood vessels and the capillary bed.

Tool kits have been made to understand the hemodynamic conditions in blood vessels. There is a framework for vascular flow models in 1D blood flow simulations [41]. This simulation assesses the hyper elasticity of vessels to understand the impact of blood flow. This model is a useful benchmark for parameters that have been studied. It shows that there is significance in understanding the dynamics of blood flow as it applies to different tissue systems. Yet, as the article is focused on the carotid artery, it presents a hyper specific application while the focus of this proposal is a more generalized framework for assessing tissue systems.

HemoSYS is another such 1D model that assesses tumor conditions through data from imaging modalities. It is a good example of the in vivo blood flow and volume data that is important to the study [42]. This article is useful in its application to multiple different tissues rather than just one condition. Yet, it lacks patient specificity which has been developed for different cancer types using computational fluid dynamics as a separate study which also uses MRI. The combination of patient / tissue specific parameters with a model such as HemoSYS can shed light into comparative differences within tissue systems. No such study has been found through the literature search. However, two key discoveries were made regarding flow simulations.

First, computational fluid dynamics in blood flow is a well-researched subject and has been conducted in various dimensions including the 4D application of space and time as dimensions.

This led to the development of several open-source software that can be used as a reference in developing the impact of blood flow from a CFD perspective[43] [44]. Two examples of open-source software are SimVascular and OpenFOAM. They both discuss the impact of flow fields such as pressure, wall shear stress, vorticity, and time. They both also have meshing models that are applicable to the computational research being conducted and can be used as a starting point to find an appropriate geometry and mesh condition for any biological tissue being researched [45]. Fig. 8 shows the general framework used for the development of CFD models in blood vessels.

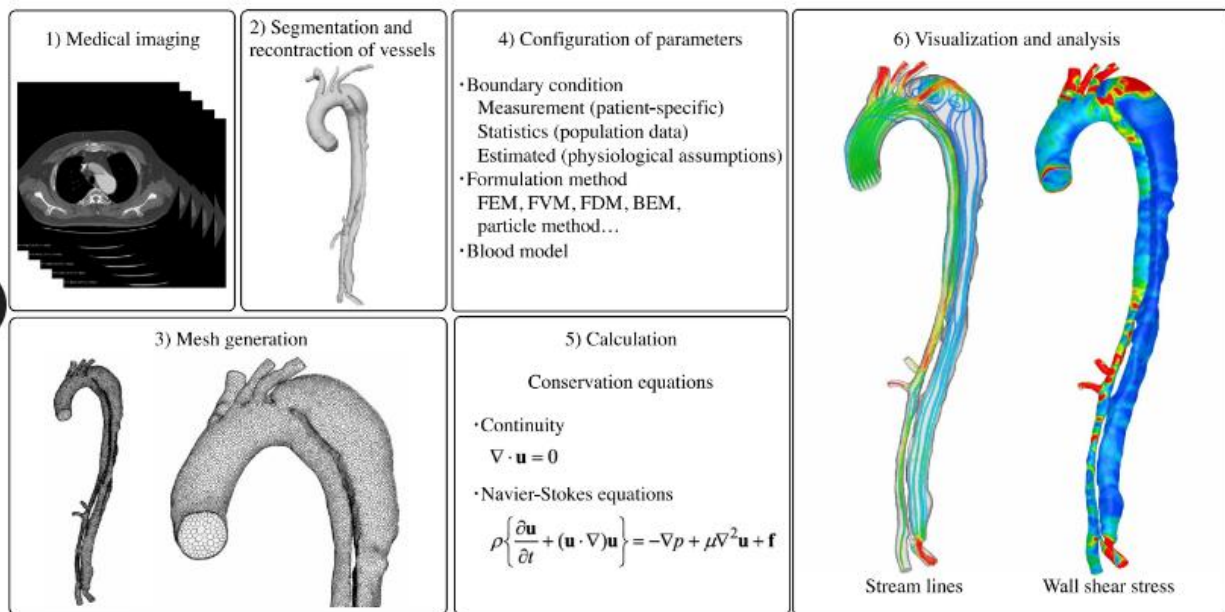


Figure 8: Framework of the CFD Procedure for Modeling Blood Flow, Vasculature, and Vascular Diseases Through Medical Imaging, reproduced from Kamada et. al [44]

Second, the impact of blood flow has been well researched in solid tumors. Mathematical research has been conducted to understand the haphazard distribution of angiogenesis and fluid flow within cancers [46]. While this research has not been expanded to include bioheat models, it is an excellent starting point to understand the level of nonuniformity in disease tissues and interstitial fluid profile (IFP).

3.4.4: Advanced Tools for Modeling and Their Pitfalls

One computational framework, AngioTool computes vascular networks in microscopic images in a quick and reproducible way. It uses the previously mentioned parameters, including branch

length, and cross section to create a segmentation analysis and skeletonization of the vessels in each tissue. The goal of this tool is to analyze vessel irregularity using image analysis techniques. The concepts of segmentation and vessel analysis parameters in this paper are useful for current research. However, the tool doesn't have any consideration of 3D tissue structure and is limited by image quality. It also doesn't incorporate heat transfer elements and is not a well-rounded approach to whole tissue analysis. Yet, the factor of the disturbance of vessels (how haphazard the vessels are) is considered in this model and can be useful to explore further [47].

Other papers have been published with regards to segmentation of 3D structures. One interesting application was the use of "convolutional neural networks for segmenting 3D in vivo multiphoton images of vasculature in Alzheimer disease mouse models"[48]. While the tissue isn't focused on a human application, the volumetric imaging of 3D vessels was used to deal with a core problem of segmentation. The neural networks described in this paper were used to create imaging segments to compare normal and abnormal physiology in mouse models. The software was packaged into DeepVess, a software that is much faster than manual annotation. The paper can be used to reference the analysis of vessel centerlines and appropriately classify unconnected vessels and segment bifurcation. The experiment is in vivo, and the open-source code may be applicable to any live tissue once parameters are modified. The primary problem to consider is that 3D imaging used may be poorly applicable to other vessel structures, so experimentation is needed to determine the effectiveness of DeepVess in human mouse models[48].

Another open-source software called VesselVio uses pre-binarized vascular data to compute 2D and 3D centerlines, segment vessels, and reports features such as volume and surface area. This document is great to assess patterns and visualize any vessel systems. Yet, it doesn't have a flow analysis so it will not be useful after determining the geometries to be used [49]. One paper used fluid simulation to discuss in vivo pressure and shear stress. It complements Vessel Vio's segmentation approach and adds a patient specific image that can transform any raw models into a flow characteristic study. The framework can be used for global optimization but is currently only available for force and pressure analysis[50].

There are also papers that analyze angiogenesis in kidney models to generate the volume of vessels, supporting previous research in angiogenesis and developing a vascularization network

focused on kidney geometry. Their flow analysis and characterization methods can be useful in the effort to perform patient-specific models and in-vivo models [51]. A learning-based algorithm was created after the previous papers to include multiple feature maps that influence the performance of a model and create evaluation metrics and simulate the ground truth. The paper used training and test method validation based on specificity, accuracy, and precision [52].

Several computational models were analyzed to determine the common assumptions within them all. The first pattern found was that cancer biology and interaction of single cell behaviors affect the full tissue simulations and environmental conditions in the selected region. Therefore, lattice and off lattice methods were used to create appropriate geometries and meshes based on how organic the structure was expected to be. Lattice methods were used for efficiently tracking organic structures, while off lattice methods were used for assessing volume and boundary-based methods. The paper also details several toolkits that can be used to select geometries and computational methods based on the research question and the biology that was selected. The following image summarizes the lattice selections and off lattice resolutions. While more details regarding modeling methods are provided in the paper, it is a good visual representation of how the geometries are visualized in each method [53].

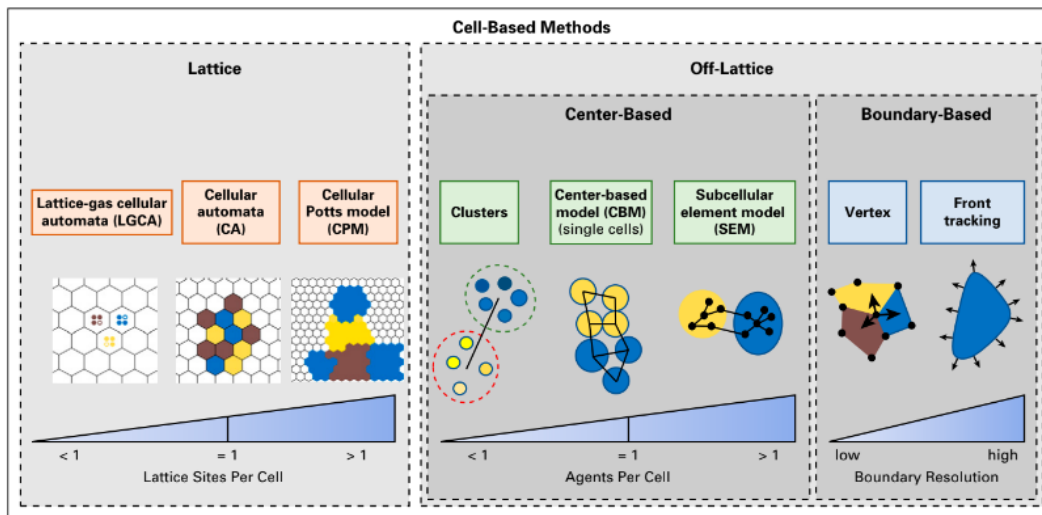


Figure 9: Computational Modeling Methods that Account for Cell, Tissue, and Organ Level Interactions, reproduced from Metzcar et. al [53]

Lastly, the properties of malignant tumors were all incorporated into the models for those that were considering both normal and abnormal tissues. The images were skeletonized into binary

forms to allow for all types of geometry to be fully characterized. The parameters that were considered in all major papers include the clustering/distribution, the average path length of the vessels, and an analysis of either nodes or branching points that indicate the major geometries. These parameters were important to the analysis of data sets from a fluid flow and heat transfer perspective [54] [55]. While more models can include both heat transfer and fluid flow, the analysis of existing computational models provided insights into the current state of the art technology, challenges, and best practices that can be used to determine the properties (particularly, the factors that affect effective thermal conductivity) of an in-vivo tissue system.

3.5 Bioheat Transfer Applications in Human Tissue

3.5.1 Forms of Heat Transfer in Humans

Various levels of temperature dependencies exist within human tissue. These are detailed within the textbook regarding the “Theory and Application of Heat Transfer within Humans”. Heat transfer occurs in cells, tissues, organs, and impacts the whole body. Whole body human computational models, cardiovascular, and respiratory models were studied. Tissue properties and calorimetry applications are included in the theory of heat transfer. Relevant findings to the study of tissues include generic thermal model for perfused tissues that were created. The models extended to in vivo temperatures. The thermal effects and heat generation due to blood vessels were also studied separately. A section of the textbook studies the effects of thermal stresses on the body, including heat induced thermoregulation and metabolic changes. This study is extremely relevant to the properties of heat transfer within the body. It is indicative of the physiological properties to be studied in the scope of this project [1].

Another important discussion is the mechanism of tissue injury in cryosurgery and ablation. The section presented in the book describes heat transfer as it applies in freezing injuries, tissue models, and discusses the biochemical reactions that happen because of varying parameters such as the cooling rate, tissue type, and duration of temperature exposure. It is important to note that all these applications of heat transfer use the same key parameters to quantify and characterize the heat transfer in various types of tissue [1]. The primary limitation of the book is that it does not focus on a whole tissue system (i.e., one that combines tissue systems which include blood vessels and may be affected by cancer).

3.5.2 Key Parameters Used in Heat Transfer in Biological Tissue

The key parameters that are used in heat transfer in biological tissue include:

- 1) Thermal conductivity: how heat travels through a given system. In this case, the focus is the thermal conductivity of a live tissue which includes blood vessel flow.
- 2) Tissue perfusion: How well fluid, typically blood, travels through the tissue.
- 3) “Specific heat: the amount of heat needed to raise the temperature of 1 gram of tissue by 1 degrees Celsius” [1]

Other parameters that are of impact include fluid flow characteristics and the geometries of the models, including vessel size and vessel density, flow velocity, viscosity, etc. Conservation laws of momentum, fluid transport, and mass transport drive the fundamental effects of blood flow with these variables. The effect of porous media and cell adhesion may be of impact in heat transfer based on the effect of transport phenomena but are excluded from this study.

Based upon the literature search, the effective thermal conductivity of a tissue system was not assessed in terms of these parameters. Research conducted by Gautherie measured the temperature of the tissue and its effective conductivity in breast cancer. The work studied tissues composed of cancer, blood flow, and normal cross sections using measurements and infrared thermography [56]. This work is the most detailed to date. Further research needs to be conducted to determine the effective thermal conductivity of tissue systems while including the effect of blood vessel development in the tissue. Such work can enhance the understanding of the impact of blood vessels at a fundamental bioheat transfer level and can have applications in angiogenesis, ablation, cancer development, or other thermally significant processes.

3.5.3: One Focused Application – Breast Cancer and its Thermal Significance

Breast cancer is an application for modeling heat transfer in tissues. The first in-patient research was conducted by Gautherie by taking measurements of the live tissue temperature [5]. The research shed light on the fact that heat transfer was significant within breast cancer. It was the basis for future heat transfer research within tissues, but the work didn't progress into later years due to ethical concerns. The experiment used long probes that were stuck into women who were in the cancer diagnosis process, which is not allowed in modern medicine. Yet, the results

regarding temperature drop, thermal changes, and metabolic heat generation within cancer were groundbreaking due to the patient-specific models that were created from this limited data set[5].

The composition of breast tissue is unique. The full breast is encased in skin and consists of a mixture of glandular epithelial cells that line the ducts of the breast, fat tissue that makes of the rest of the tissues, and fibrous tissue. Fat composition often increases with age. The anatomy of a healthy breast is given in Fig. 10 [57].

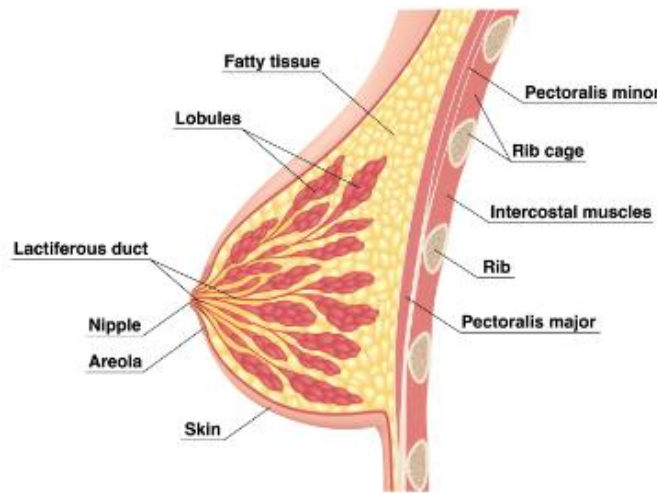


Figure 10: Anatomy of a Healthy Breast, reproduced from Camilleri et.al. [57]

Breast tumor spreads through this tissue using the infiltrative cancer methods discussed earlier in literature. It undergoes angiogenesis, or the development of blood vessels, that is common in several types of solid cancers. The properties of breast tissue have been used to model and measure the changes that happen during this process. The density of blood, ρ_{blood} , is 1050 kg/m^3 . The specific heat of blood is 3617 J/kgK . The thermal conductivity of blood, k_b , was 0.52 W/mK , and viscosity is 4.5 mPa [57] [58].

Upon further research, fat tissue was chosen in this experiment as it has the most straightforward composition and measured values found in literature. The tissue density was found to be roughly 1 g/cm^3 , thermal conductivity, k , was 0.21 W/mK , and specific heat was 2350 J/kgK for soft tissue. There was no singular value for fat tissue as it changed between the several experiments. Yet, the values were ensured to be within the thermal and physiological properties reviewed by Camilleri and are based on generalized fat tissue, and were verified via a population data base

from the ‘ITIS Foundation’, which is a Swiss nonprofit research organization for technologies in society [57] [59] [60]. This tissue type was measured in Gautherie’s experimentation along with the glandular and fibrous tissues in the breast as the patients in the study underwent treatment and diagnosis.

The parameters that affected the breast model were also isolated using infrared technology and were used to support the detection of early breast cancer. Infrared screening became a new, inexpensive, and non-invasive method that was used to identify cancerous changes in women. Early detection methods developed with the advent of better cameras, improved numerical simulation, and artificial intelligence models that were trained to study the distinguishing parameters of cancer. Results from Gutierrez show the results of infrared imaging and an inverse heat transfer computational (IRI) model, demonstrating high accuracy of cancer detection methodology in Fig. 11 [61].

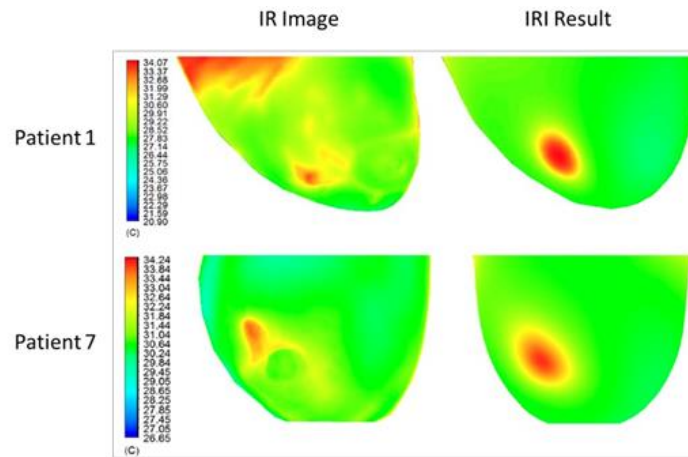


Figure 11: Infrared Imaging and IRI Numerical Engine Computation of the Cancer Location using Modeling Methods, reproduced from Gutierrez [61]

The mathematical models that developed in the late 1900s accurately calculated the thermal energy equilibrium in the body, conservation of energy in tissues, and the impact of blood and discrete vessels in the tissue models. The calculations were applied over 2D and 3D reference frames of an ideal (hemispherical) breast model at first. The transition to patient specific modeling as shown in Fig. 11 led to forward and inverse computational methods that had detection accuracies within 80 and 95% [62].

All these models used an assumed conductivity factor and focused on creating neural networks, variance functions, etc. Table 1 is attached below detailing the main mathematical models used in breast cancer applications in chronological order. The models are based on bioheat transfer equations, of which the relevant models are discussed further in the upcoming sections.

Table 1: Mathematical Equations Historically used in Breast Cancer Thermal Models, reproduced from Mashekova et. al [62]

Modeling Method or Author	Meaning
Pennes' bioheat equation, 1948	Uses Fourier's law of conduction to determine thermal equilibrium of breast cancer
Mitchell and Myers, 1968	Discrete vessel approach accounting for a dominant countercurrent flow in a tissue cross section with boundary conditions
Keller and Seiler, 1971	Extension of Myers with improved perfusion modeling
Wulff, 1974	Mathematical equilibrium of blood and tissues, and metabolic heat transfer
Chen and Holmes, 1980	Discrete vessel model describing the heat exchange between a single vessel and its surrounding tissue
Weinbaum and Jiji, Lemons, 1984-1992	Describes effective conductivity in vasculature, countercurrent exchange, and distribution of heat transfer

3.6 Bioheat Transfer Models Used in Computation

The bioheat transfer models mentioned in Table 1 to solve for the heat transfer within breast cancer are derived from general bioheat transfer theory of vascular tissue. The common models, including those listed above, are assessed for their pros and cons. The following information is derived from Etehadtavakol's et. al's 'Survey of Numerical Bioheat Transfer Modelling' [2].

3.6.1 Pennes' Bioheat Transfer Equation

Most thermal systems are assessed via an energy balance. Blood was recognized very early on as a thermoregulatory system that impacted tissues. Pennes proposed his bioheat transfer equation (Eqn. 5) involving the impact of both blood and heat generation on a tissue [2]:

$$\rho c \frac{\partial T_t}{\partial t} = k_t \nabla^2 T_t + q_b + q_{met} \text{ (Eqn. 5)}$$

Here “ t and T are the time and temperature, q_{met} is the metabolic heat, and q_b is heat transfer due to blood” [2]. Then, ρ signifies tissue density and c is the specific heat of the tissue. This model tackled the most challenging concept of perfusion in the human body and represented it in a simple form. The underlying assumption was that the “tissue was perfused via capillaries, that are supplied by arteries and drained by veins” [2].

While this model was a great starting point for bioheat modeling and fit experimental data easily, it had major flaws in its applications. First, the blood flow direction was not included in this research. The counter current flows created by artery-vein pairs in most normal tissues were not modeled until later. The other limitation of this model is in the way that it accounts for the temperature of the blood. Arteries experience significant slowing of blood flow and face rapid increase in conductivity as the surface area of vessels increases with decreasing diameter [2]. This effect is much more pronounced in vessels that are within or border abnormal tissues that generate heat. Blood vessels close to the capillary beds don't impact heat exchange and must be in the range of thermally significant geometry. This effect is impossible to consider as the local vascular geometry is ignored. Instead, the model assumes that arterial blood flow “bathes” the tissue everywhere and maintains the same temperature, which is incorrect. This model can only be used in large sections where temperature averages out within the cross section and any other variances reach equilibrium, as only variable in the equation is the tissue temperature [3].

3.6.2 Other Bioheat Transfer Models

Newer bioheat transfer models were developed in reaction to the Penne's equation. Wulff's model introduced blood flow direction and improved the involvement of countercurrent flow pairs in most arteries. This work moved away from the capillary bed suggestion and accounted for orientation impacts. Yet, it strongly suggested that tissues and blood were in thermal equilibrium, which is not always the case.

Models such as Chen and Holmes focused on adapting the model for various vasculature sizes, while Eriksson analyzed countercurrent flow in smaller arteries and veins. These equations became increasingly complicated to detail the vascular information. Some of these models were heavily based on measurements and others had multiple equations. Other models used control structures including dual phase lag models, self-tuning controllers for thermal regulation, and

finite element heat transfer to consider elemental and porous effects that were previously neglected for the sake of simplicity [2].

Weinbaum's model was particularly interesting as it was the first of its kind to create an improvement factor to express the thermal effect of blood on tissues: effective thermal conductivity, k_{eff} . This parameter depended on two factors, the local perfusion rate and the vessel geometry. The authors also simplified the heat conduction in a tissue to include two things, 1) heat loss from arteries due to perfusion and 2) dominance of heat conduction in tissues with a large ratio of vessel spacing to diameter (described as a shape factor, the Peclet number). Weinbaum's equation is described by Eqn. 6, as reproduced from Weinbaum and Jiji [10]:

$$\frac{n\pi^2 a k_b}{4k_t} Pe \left[\frac{2gPe}{\sigma \bar{u}} \frac{dT_t}{ds} - \frac{d}{ds} \left(\frac{aPe}{\sigma} \frac{dT_t}{ds} \right) \right] = \nabla \cdot (k_t \nabla T_t) + q_m, \quad Pe = \frac{2a(\rho c)_b \bar{u}}{k_b} \quad (\text{Eqn. 6})$$

The Pe is the Peclet number, k signifies thermal conductivity of the tissue (subscript t) or blood (subscript a). The n is the number of vessels, a is the vessel diameter, and T signifies temperature. The c is the specific heat, q_m remains metabolic heat generation, and u is the blood flow velocity. Lastly, σ is the shape factor, a simple ratio of the vessel spacing to vessel diameter [10].

The limitation of this model is that the countercurrent flow setup it has is applicable near skin layers. Deeper tissue layers have a capillary bleed off phenomena and the vessel geometries are more defined by pressure flows, creating complexities when this method is applied to cancers or organ like tissues [3]. With this limitation, the question arises. How can the model be applied to deeper tissues? For this, it would be useful to know how geometry of blood vessels and its flow impacts the effective thermal conductivity, which "can be defined from any known heat flow and temperature difference" [12] as

$$k_{eff} = \frac{q \Delta x}{A \Delta T} \quad (\text{Eqn. 7})$$

In this equation, k_{eff} is the effective thermal conductivity, A is the area defined by the heat flow, q is the heat flux, and x is the depth of the tissues where there is a difference in temperature, T. This equation is derived using Fourier's law of conduction. Further research into the impact of geometry on conductivity of vivo tissues is needed as this topic has had little consideration in

experiment and theory. The aim of this study is to find the parameters that define effective thermal conductivity and heat flow in tissues with blood vessels.

4.0 OBJECTIVES OF THE PROPOSED WORK

The impact of bioheat transfer is well researched in normal and abnormal tissues. The development of cancer, thermal radiation, or ablative surgery are common causes of change in tissue heat signatures. Gautherie's research on breast cancer patients demonstrated that heat transfer was significant among the tissues adjacent to the cancer mass [5]. Angiogenesis (the development of blood vessels) was identified as a key factor for the elevated heat flow and clearly correlated with an increase in effective thermal conductivity, creating a pivotal study regarding bioheat transfer in live tissues [56].

While the impact of blood vessels has been modeled over a large tissue cross section, measuring the effect of each individual vessel is challenging due to their small scale. The first objective of this research is to understand how vascular geometry changes the effective thermal conductivity in live tissues. The second objective is to create a simplified model of the tissue with a blood vessel to justify the substitution of effective thermal conductivity as an equivalent. The effect of the following factors will be determined using computational fluid dynamics (CFD) simulations:

- Vessel Diameter
- Vessel Length
- Velocity of blood flow
- Validation of the use of effective thermal conductivity

5.0 METHODS

5.1 Theoretical Background and Key Assumptions

Effective thermal conductivity (k_{eff}) is defined as the overall thermal conductivity of any geometry, which may contain multiple materials. The k_{eff} was analyzed in a tissue composite with one blood vessel to understand how each vascular parameter selected (vessel diameter, length, and flow velocity) affects the tissue. The properties used were that of in vivo (live) tissue to understand how a tissue composite functions in the human body where vasculature is embedded in it.

The study was first conducted in 2D with the initial goal of saving computational time, as parametric studies take significant resources. Human vasculature is a 3D geometry, so the flow regimes were matched by ensuring the 2D simulations have the Reynold's number value as a corresponding 3D flow. Next, a 3D version of the geometry was analyzed with the same parameters. The values were compared to the 2D outcomes.

The simulation was tested with added vasculature to get preliminary results for the impact of multiple vessel flows. The pressure drop, temperature drop, and the use of Newtonian fluid properties for blood (a non-Newtonian fluid) were validated. The results were also compared with Gautherie's effective thermal conductivity measurements for accuracy, as a case study on the use and validity of effective thermal conductivity.

The Design Modeler software was used to generate geometry in each case. The processing was conducted in Ansys Fluent, where boundary conditions were set up. The parametric study was conducted by modifying the variables in the Ansys Workbench module that contains the project.

The flow conditions are dictated by anatomy and physiology. The model does not incorporate pulsatile and reverse flow as the blood flow in the selected tissues is far from the heart. The flow is steady state and laminar, as found in arteries that are far away from the heart. There are also no early stage turbulence or cardiac effects to consider [12]. The flow parameters and vessel geometries that are considered in this simulation are all relevant to medium and small arteries, arterioles, and capillaries. The vessels themselves are assumed to be perfectly circular for the 3D simulation and of uniform diameter for the 2D. The purpose of simplifying the geometry is to mitigate surface roughness effects and other topology issues that may impede CFD simulations.

There is no external heat transfer in the system as it is assumed to be isolated in the human body. The contact resistances between the walls are also assumed to be negligible as the vessels have a very similar conductivity to that of the surrounding tissue. It is assumed that there is internal boundary continuity and that there are no gaps between the resistance chains in the simulation. That is, there are no extracellular fluids or dead tissues present. Additionally, heat transport occurs in thermally significant blood vessels that are capillaries and arterioles [12]. The analysis will assess the impact of vasculature larger than 80 micrometers and smaller than 5 mm, using the velocity profiles available.

The vascular dimensions are shown in the table below, where the ranges of inlet velocity, vessel diameter, and length were varied during the analysis using anatomical minimum and maximum ranges for the four types of vessels found in soft tissue: capillaries, arterioles, small arteries, and artery branches. Therefore, the smallest vessel has a diameter of 0.5 mm, a length of 1 mm, and an inlet velocity of 0.05 cm/s. The largest artery branch considered is a 5mm vessel, with a length of 54 mm and 25 cm/s [9] [63] [58]. The parametric analysis accounts for the anatomical and flow conditions of the vessels between these two ranges, while keeping other parameters constant.

Table 2: Anatomical dimensions and flow conditions of the parametrized vessels [9] [16] [58]

Type of vessel	Diameter [mm]	Linear Velocity [cm/s]	Length [cm]
Artery Branches	4-5	10 - 40	1.4-2.8
Small Arteries	2.5-4	10 - 40	1-2.2
Arterioles	1-2.5	Less than 20	0.6-1.7
Capillaries	0.5-1	0.05 - 0.1	0.3-1.3

The properties of fluids and tissues were determined by finding values used in existing physics simulations and anatomy papers, as given in Table 3 below and given in the literature review section. The temperature of blood was found to be 311 K and the internal body temperature of healthy tissue 310 K [57] [6].

Table 3: Material Properties of Blood and Fat Tissue Used in Simulation [57] [58] [59] [60]

Property	Units	Blood	Fat Tissue
Density, ρ	Kg/m ³	1050	1000
Thermal conductivity, k	W/mK	0.52	0.21
Specific heat, c_p	J/kgK	3617	2348
Viscosity	mPa-s	4.5	-

These parameters are studied on a cross section that borders an abnormal tissue. Therefore, the cross section has a constant temperature condition on its top wall. Such conditions are generated by abnormal generation of heat due to malignancy, during ablative surgeries, and radiative heat treatment among other procedures. The computational results were validated using Gautherie, who has measurements of the selected fat tissue in his research. Further details of the computational domain are detailed in the next section.

5.2 Computational Domain and Boundary Conditions

The 2D computational domain in Fig. 12 shows the tissue composite where the blood vessel diameter (d_{vessel}) and tissue thicknesses (t_{tissue}) are equal in this study. This creates a tissue matrix where the properties of the tissue can be assessed for an embedded vessel. The blood vessel is assumed to have no loss of blood or significant exchange of outside fluids. Additionally, the top wall has a heat source at 333 K (T_1), which is a high temperature condition to simulate tissue that is different from normal cross sections. The bottom wall is healthy tissue at the normal body temperature of 310 K (T_2), as given in the literature. This composite simulates vessels that are adjacent to the center of a bioheat source, whether mechanically applied or generated within the body. These walls are extended by default in the z direction by one unit length (1 meter) during the calculation process in the Ansys Fluent software. The conditions create the resistance diagram shown on the right. The tissue and blood vessel properties and dimensions are based on data from accepted hemodynamics research as detailed in the theoretical background section. The three parameters that are varied are the diameter of the vessel, the inlet velocity of blood flow, and the length of the blood vessel. These are denoted with a rectangular box labelled 'P' for clarity.

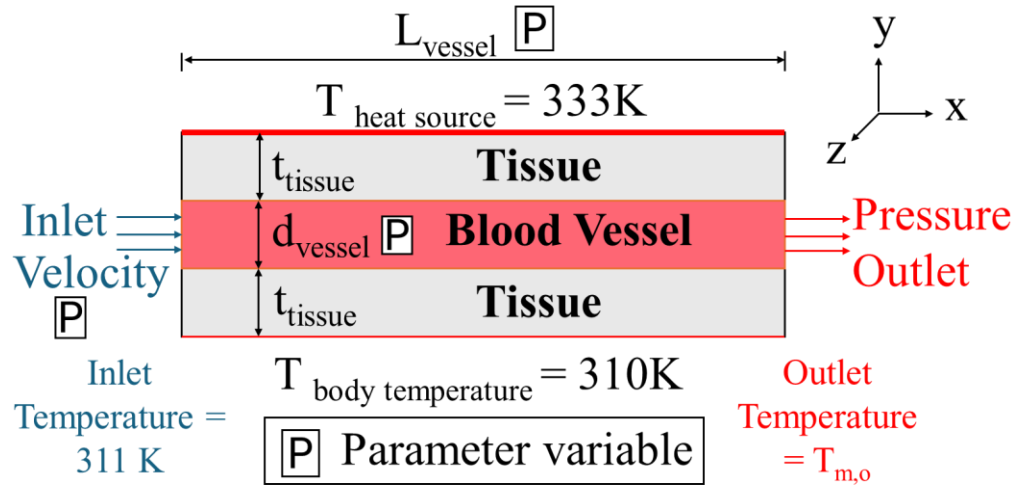


Figure 12: Overview of the 2D tissue composite, with parametrized variables labeled and a resistance diagram along the direction of heat flow

The 3D version of the simulations modifies the cross sectional 2D geometry to a tissue composite that one can find in the human body. The computational domain is given in Fig. 13, where the vessel is embedded in a square cross section. This square shape was chosen to decrease any topology issues that can occur while generating the geometry in Ansys Fluent. It also simplifies computation by keeping the geometry symmetrical on the inlet and outlet faces. If the tissue was instead embedded in a circular cross section, the geometry would have to be split down the middle, creating several topology issues in solving the problem. The d_{vessel} remains equal to the t_{tissue} measurements, and the analyzed parameters of length, diameter, and inlet velocity remain the focus of the simulation. The heat source and body temperature remain the same as the 2D geometry. The resistance diagram in the direction of heat flow along the y axis remains the same as in Figure 12.

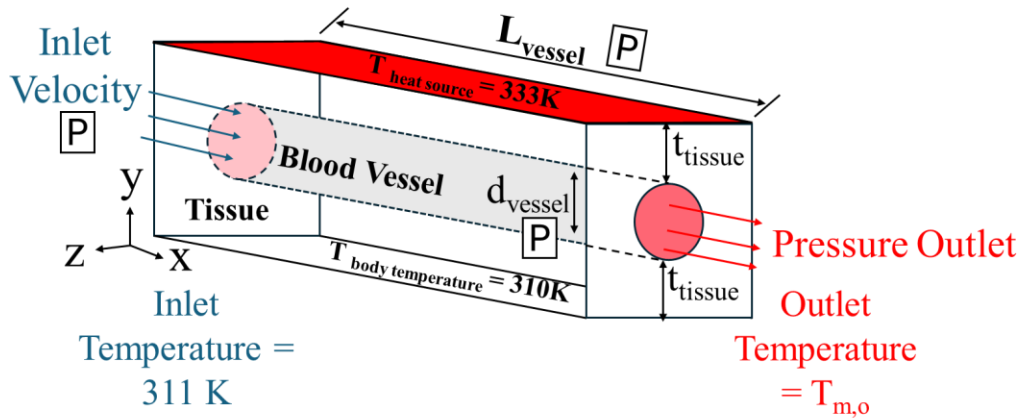


Figure 13: Overview of the 3D tissue composite, with parametrized variables labeled

The boundary conditions for the computational geometry are shown in Fig. 12 and 13. There following is a list of the conditions:

1. a constant temperature source on the top wall of 333 K
2. a constant normal human body internal temperature on the bottom wall of 310 K,
3. an inlet velocity dictated by laminar flow.
4. The blood vessel exit is a pressure outlet with no backflow in all cases.

This setup creates a good differential between the top and bottom wall temperatures and yields a high resolution temperature profile. The relevant equations for these boundary conditions are given in section 5.4. The metric unit system was used throughout this workflow.

5.3 Computational Mesh

The computational mesh analysis characteristics for the smallest 2D cross section are given in Table 4. This geometry was chosen as accounting for the smallest geometry will ensure that the larger parametric geometries will have accurate results. The four meshes that were chosen are given in the table. A picture of the fine computational mesh is given in Fig. 14. The green section of the mesh the fluid from the blood flow with the inlet and outlet shown in blue and red respectively. This is shown for additional clarity on the meshing settings that differentiate each material in the computational domain. Higher resolutions were used at the boundary of the fluid and within the fluid body to create better results across the materials as inflation layer settings

were not available for 2D geometries. Additionally, the share topology settings are used to create a cohesive geometry where the tissue and blood have proper contact effects.

Table 4: Computational Mesh Characteristics for the 4 Mesh Types in 2D Simulation

Mesh Name	Element Size [mm]	Number of Computational Cells
Coarse	0.5	1008
Medium	0.1	4008
Fine	0.09	9250
Super Fine	0.05	13694

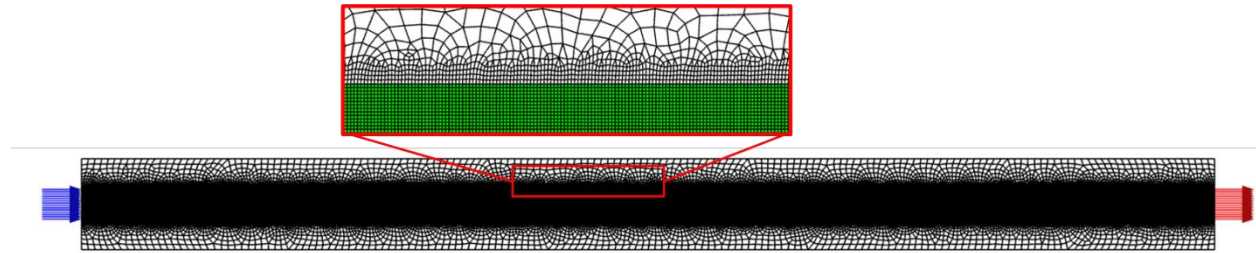


Figure 14: Picture of Fine Computational Mesh

The 3D mesh sensitivity analysis was also conducted with four meshes as shown in Table 5. Once again, the mesh was created to have good meshing characteristics for the smallest geometry (shown in Fig. 15) such that it works for any larger parametric model. The model was created by generating each of the bodies, solid tissue and fluid blood, to the appropriate sizing. Then, the topology was shared between each body and inflation layers were created between the boundary of blood vessel and tissue to increase the accuracy of calculation near the contact regions. Once again, the fluid body was created with a higher resolution to visualize the effect of blood flow.

Table 5: Computational Mesh Characteristics for the 4 Mesh Types in 3D Simulation

Mesh Name	Element Size [mm]	Number of Computational Cells
Coarse	0.2	191933
Medium	0.12	207100
Fine	0.10	2438465
Super Fine	0.05	5036516

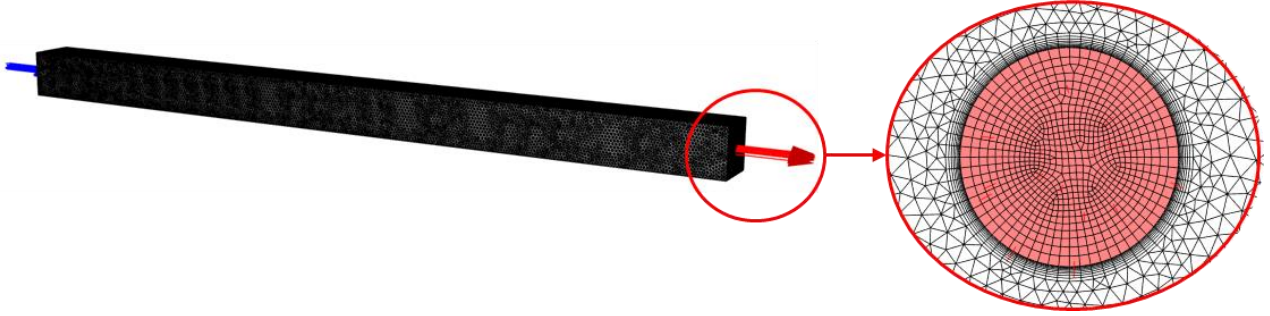


Figure 15: Picture of Fine Computational Mesh, with inflation layers and smaller fluid body sizing displayed

5.4 Governing Equations

The following equations were derived from standard heat transfer theory from Incropera et. al. and microfluidics theory from Kandlikar et. al. [64] [65]. The steady energy equation with heat diffusion and no heat generation is the primary driver of the simulations as shown in Eqn. 8 [64]:

$$\rho c_p u \frac{\partial T}{\partial x} + \rho c_p v \frac{\partial T}{\partial y} + \rho c_p w \frac{\partial T}{\partial z} = \frac{\partial}{\partial x} \left(k \frac{\partial T}{\partial x} \right) + \frac{\partial}{\partial y} \left(k \frac{\partial T}{\partial y} \right) + \frac{\partial}{\partial z} \left(k \frac{\partial T}{\partial z} \right) \quad (\text{Eqn. 8})$$

This equation accounts for heat flow in all 6 directions of a fundamental element. In the case above, the heat transfer occurs through the y direction of the computational domain. The fluid flow is shown to be symmetrical across the x-z plane (for the 2D computations), and across the y-z plane (for the 2D and 3D computations).

Therefore, the advection terms and diffusion terms are used in the y direction for the purpose of the calculations. The equation simplifies to

$$\rho c_p u \frac{\partial T}{\partial y} = \frac{\partial}{\partial y} \left(k \frac{\partial T}{\partial y} \right) \quad (\text{Eqn. 8, simplified})$$

The u,v,w signifies velocity (advection) in the x, y, and z directions. The unit analysis for this equation is:

$$\frac{kg}{m^3} \frac{J}{kgK} \frac{K}{m} = \frac{\partial}{\partial y} \left(\frac{W}{mK} \frac{K}{m} \right) = \frac{\partial}{\partial y} \left(\frac{W}{m^2} \right) = \frac{W}{m^3} \text{ (Eqn. 9)}$$

Another governing equation is the conservation of mass, where the density is constant. It is given by the equation [64]

$$\nabla \cdot (\rho \vec{V}) = \rho \left[\frac{\partial u}{\partial x} + \frac{\partial v}{\partial y} + \frac{\partial w}{\partial z} \right] = 0 \text{ (Eqn. 10)}$$

The unit analysis for this equation is

$$\frac{kg}{m^3} \left[\frac{m}{s} + \frac{m}{s} + \frac{m}{s} \right] = 0 \text{ (Eqn. 11)}$$

The Navier Stokes equation conservation of momentum for incompressible flow and a constant density is valid for the flow through the blood vessel in this simulation. It is given below for flow along the x direction (as seen in the computational domain section) [64]:

$$\rho \left[\frac{\partial u}{\partial t} + u \frac{\partial u}{\partial x} + v \frac{\partial v}{\partial y} + w \frac{\partial w}{\partial z} \right] = - \frac{\partial p}{\partial x} + \mu \left(\frac{\partial^2 u}{\partial x^2} + \frac{\partial^2 u}{\partial y^2} + \frac{\partial^2 u}{\partial z^2} \right) + \rho g_x + F_x \text{ (Eqn. 12)}$$

The system does not have any applied forces or gravitational forces (the elevation is assumed to be 0 in this system). There are no changes in density. The velocity is constant throughout.

Therefore, the equation simplifies to

$$\rho \left[u \frac{\partial u}{\partial x} + v \frac{\partial v}{\partial y} + w \frac{\partial w}{\partial z} \right] = \mu \left(\frac{\partial^2 u}{\partial x^2} + \frac{\partial^2 u}{\partial y^2} + \frac{\partial^2 u}{\partial z^2} \right) \text{ (Eqn. 12, simplified)}$$

The unit analysis is given below.

$$\frac{kg}{m^3} \left[\frac{m^2}{s^2} + \frac{m^2}{s^2} + \frac{m^2}{s^2} \right] = \frac{k}{m^2 s} \left[\frac{m}{s} + \frac{m}{s} + \frac{m}{s} \right] = \frac{kg}{ms^2} \text{ (Eqn. 13)}$$

The effective thermal conductivity output is part of the governing equation for conductivity as shown in Eqn. 14. It is derived from conduction equations used within fundamental heat transfer theory in Incropera et. al [64].

$$\frac{q}{A} = k_{eff} \frac{\Delta T}{\Delta x} \text{ (Eqn. 14)}$$

The unit analysis is shown:

$$\frac{W}{m^3} = \frac{W}{m^2 K} \frac{K}{m} \text{ (Eqn. 15)}$$

The Reynold's number was used to derive the 2D velocity of flow that equals the 3D velocity using the following equation as follows [65]:

$$Re_{2D} = Re_{3D} = \frac{\rho V D_h}{\mu} \text{ (Eqn. 16)}$$

Here, V is the flow velocity, μ is the viscosity of blood, and ρ is the density of blood.

$$\frac{\rho V_{2D} D_{h,2D}}{\mu} = \frac{\rho V_{3D} D_{h,3D}}{\mu} \text{ (Eqn. 16, simplification step 1)}$$

$$\frac{\rho V_{2D} D_{h,2D}}{\mu} = \frac{\rho V_{3D} D_{h,3D}}{\mu} \text{ (Eqn. 16, simplification step 2)}$$

$$V_{2D} D_h = V_{3D} D_{h,3D} \text{ (Eqn, 16, simplification step 3)}$$

The hydraulic diameter was calculated using Eqn. 17 [65].

$$D_h = 4 * \text{Area}/\text{Perimeter} \text{ (Eqn. 17)}$$

Where the area and perimeter account for the wetted surfaces of a rectangular geometry of the channel with a depth of 1m. The channel width in 2D is equal to what would be the vessel diameter in 3D.

For parallel plate flow (which represents the 2D) was found to be $D_{h,2d} = 2D$, and the $D_{h,3D} = 3D$, where D is the diameter of the channel. Therefore, the final equation for 2D velocity in comparison to 3D velocity is:

$$V_{2D} = \frac{V_{3D}}{2} \text{ (Eqn. 16 final derivation)}$$

Therefore, the flow regime (laminar flow with the same properties) of every 2D case is comparable to a 3D case at half the 3D velocity. This was accounted for in the simulations. Lastly, the boundary conditions are listed below in equation form.

$$T_{top} = 333 \text{ K for all cases} \text{ (Eqn. 18)}$$

$$T_{bottom} = 310 \text{ K for all cases} \text{ (Eqn. 19)}$$

$$V_{inlet} = u_{\infty} \text{ and } T_{inlet} = 311 \text{ K (Eqn. 20)}$$

5.5 Ansys Customization

User defined functions and customization variables not used in the parametric experiments. All equations that solve the simulation conditions are detailed in Sections 5.4. The primary customization method used was parametric variables created for the pipe diameter and length to change the geometry automatically in Design Modeler. Additionally, a parametric variable was assigned to the inlet velocity condition in Ansys Fluent to change the input. These variables were controlled through Ansys Workbench as they yielded the primary output of the heat flux on the top wall.

The effect of Newtonian versus non Newtonian viscosity models was tested to validate the use of a constant viscosity parameter in the blood flow. The Casson and the Power Law

models (Eqn. 3 and 4) were used to evaluate the impact of viscosity on the heat transfer within the tissue model. These two equations were input into the viscosity of the fluid in Ansys via a ‘DEFINE PROFILE’ user defined function. The results of the two models were compared to the Newtonian simulations conducted which were input into Ansys as the function for viscosity.

6.0 RESULTS AND DISCUSSION

6.1 Mesh Sensitivity Analysis Outcomes

The mesh sensitivity analysis showed that a decrease in element size led to an increase in the computational cells and a higher resolution as expected. The results in Table 6 prove mesh independence after the mesh sensitivity analysis reaches the fine resolution with an element size of 0.00009 m.

The key parameter that is assessed is the heat flux across the top wall of the system. This output is part of the effective thermal conductivity analysis and therefore was chosen to prove independence. As seen, the fine and super fine resolutions yield the closest variation in results. The fine mesh was picked as it combines the optimal computational time with the highest resolution. These meshes were tested on the smallest diameter and velocity cases of the parametric study (vessel diameter of 0.5 mm and velocity of 0.05 cm/s) as the resolution remains accurate for larger geometries if the smallest element size needed is accounted for.

Table 6: Mesh Sensitivity Analysis Results for the 4 Mesh Types in 2D Simulation

Mesh Name	Number of Computational Cells	Top Wall Heat Flux [W]
Coarse	1008	69.52
Medium	4008	72.27
Fine	9250	71.71
Super Fine	13694	71.72

The results of the 3D mesh sensitivity analysis were like the 2D counterparts. Once again, the fine mesh was used to balance the computational time and resolution. Mesh independence was proven by the results in Table 7.

Table 7: Mesh Sensitivity Analysis Results for the 4 Mesh Types in 3D Simulation

Mesh Name	Number of Computational Cells	Top Wall Heat Flux [W]
Coarse	191933	1.242308
Medium	207100	1.242226
Fine	2438465	1.240070
Super Fine	5036516	1.242032

6.2 Results of Verification and Validation

Fluid Flow Characteristics: Pressure Drop

The fluid flow characteristics of the simulations were validated by conducting a pressure drop analysis across the channels. The 2D geometry in Ansys inherently has a parallel plate flow configuration during the simulation as it extends the walls in the “z” direction by one unit length, which is 1 meter. This implies that there is effectively an infinite top boundary for the heat source. The pressure drop equations were adjusted accordingly to ensure that the pressure drop in this geometry is calculated appropriately.

The validation was conducted for two cases, first for a singular blood vessel with a diameter of 0.5 mm, flow velocity of 0.1 cm/s, and a length of 10 cm. The second case had a geometry of 2mm, flow velocity of 5 cm/s, and a length of 15 cm.

First, the D_h was calculated using Equation 17. Then, Reynold’s number, Re , was calculated and verified to be laminar using Eqn. 16. The frictional factor, f , was calculated via using the Poisselle’s number (Po) for flat channels, reproduced from Kandlikar et. al [65]:

$$Po = fRe, \text{ where } Po = 24 \text{ for flat channels} \quad (\text{Eqn. 21})$$

Lastly, the pressure drop for 2D channels, ΔP , was calculated using the general equation for pressure drop from Kandlikar et. al [65]. The variable L is the length of the blood vessel.

$$\Delta P = \frac{2f\rho V^2 L}{D_h} \quad (\text{Eqn. 22})$$

The outcome of the calculations is given in Table 8:

Table 8: Pressure Drop Validation for 2D Geometry

Calculated Parameter	Case 1: D = 0.5 mm, V= 0.1 cm/s, L = 10 cm	Case 2: D = 2 mm, V = 5 cm/s, L =15 cm
Eqn. 17: D_h [m]	0.001	0.00399
Eqn. 16: Re [---]	0.233	46.6
Eqn. 21: f [---]	103	0.515
Eqn. 22: ΔP [Pa]	2.16	101.66
Experimental (Ansys Fluent): ΔP [Pa]	2.24	105.94
Percent Difference [%]	3.60	4.21

As seen in Table 8, there is less than a 5% difference between the theoretical and experimental values for the 2D case. The difference is negligible for the purpose of this parametric study and shows good agreement between the expected outcomes. One major cause of potential error is that entrance effects were included in the 2D calculation as the derivation of an entrance effect formula for flat channels is both time consuming and differs from the focus of the goals of this parametric experiment. This phenomenon is also the reason that case 2 has a slightly larger error, as the entrance effects are more prominent for higher velocity laminar flows. Yet, the pressure drop validation shows that the flow parameters are functioning as expected for the materials and geometry in this study.

The pressure drop validation was also conducted for the 3D geometries. The entrance effects were calculated using accepted formulas and excluded from the experimental pressure drop so that the flow parameters remain true to the purpose of validating ΔP in steady state pipe. The process of validation is shown below.

First, the hydraulic diameter, D_h , is equal to the diameter, D , for circular pipes. So, Eqn. 17 was simplified to, as tabulated in Kandlikar et. al [65].

$$D_h = D \text{ (Eqn. 17, for circular pipes)}$$

Then, Eqn. 16 was used to calculate Reynold's number. The friction factor was found using Eqn. 20, with the Poiseuille's number modified to account for circular pipe flow, as given in Kandlikar et. al [65].

$$Po = fRe, \text{ where } Po = 64 \text{ for circular pipe flow (Eqn. 21, modified)}$$

The pressure drop in pipes was calculated using the general pressure drop formula in Eqn. 22 and validated successfully in every case against Darcy’s equation for pressure drop. The results of the pressure drop calculations matched each other, showing that the methods used were mathematically correct.

The length of the entrance effects was calculated to neglect such effects from the experimental pressure drop to increase the accuracy of the comparison between the theoretical and experimental values, as given in Kandlikar et. al [65].

$$x_{entrance} = 0.05DRe, \text{ for a circular pipe (Eqn. 23)}$$

The outcome of the pressure drop calculations for the 3D cases are shown in Table 9.

Table 9: Pressure Drop Validation for 3D Geometry

Calculated Parameter	Case 1: D = 0.5 mm, V= 0.2 cm/s, L = 10 cm	Case 2: D = 2 mm, V = 10 cm/s, L =15 cm
Eqn. 17: D_h [m]	0.0005	0.002
Eqn. 16: Re [---]	0.233	46.6
Eqn. 21: f [---]	274	1.37
Eqn. 22: ΔP [Pa]	172.8	540
Eqn. 23: $x_{entrance}$ [cm]	0.00058	0.466
Simulated (Ansys Fluent): ΔP [Pa]	174.53	543.76
Percent Difference [%]	1.00	0.70

The results in Table 9 indicate that the use of entrance effects in comparing the experimental and theoretical data significantly decrease the error in comparison 2D results and are a significant part of the contribution to the error as predicted. The 3D geometry provides the best results for flow parameter validation and should therefore be considered seriously.

One notable difference between the 2D and the 3D geometries was that the friction factor and pressure drop were significantly different even when the cases had the same Reynold’s number that resulted in a matching flow regime. This is natural due to the plate flow conditions in 2D that contrast the improved pressure drop and flow seen in the 3D cases. The conclusion from the

differences in flow characteristics is that 2D geometry may be considered a planar modeling alternative used to analyze the patterns in parameters and decrease computational time for this internal flow case. Yet, it cannot match the exact flow parameters of a 3D geometry and should be used with caution.

Thermal Characteristics: Thermal Conductivity and Outlet Temperature Modeling

The thermal property validation of the 2D geometry was more challenging than expected. The temperature drop value of the geometry shown in Fig. 12 requires the derivation of a formula for parallel plate flow with two different plate temperatures. This task was not valuable in proving the main hypothesis of this experiment. Therefore, the concept of effective thermal conductivity was validated against Gautherie's calculations as given in the results below.

The heat conduction equation [64] is defined by Eqn. 14 is expanded to be

$$\frac{q}{A} = \frac{k_{eff}(T_{hot} - T_{cold})}{t} \text{ (Eqn. 14, expanded)}$$

Here, q is the heat flow rate, A is the cross sectional surface area perpendicular to the heat flow rate, T_{hot} is the hot surface from which heat is flowing, and T_{cold} is the cold surface to which heat is flowing. Lastly, t is the thickness of the analyzed cross section. This equation can be used to calculate the effective thermal conductivity for any cross section. In the case of the 2D geometry, The heat flows as shown in Fig. 16 due to the way Ansys interprets the computational geometry.

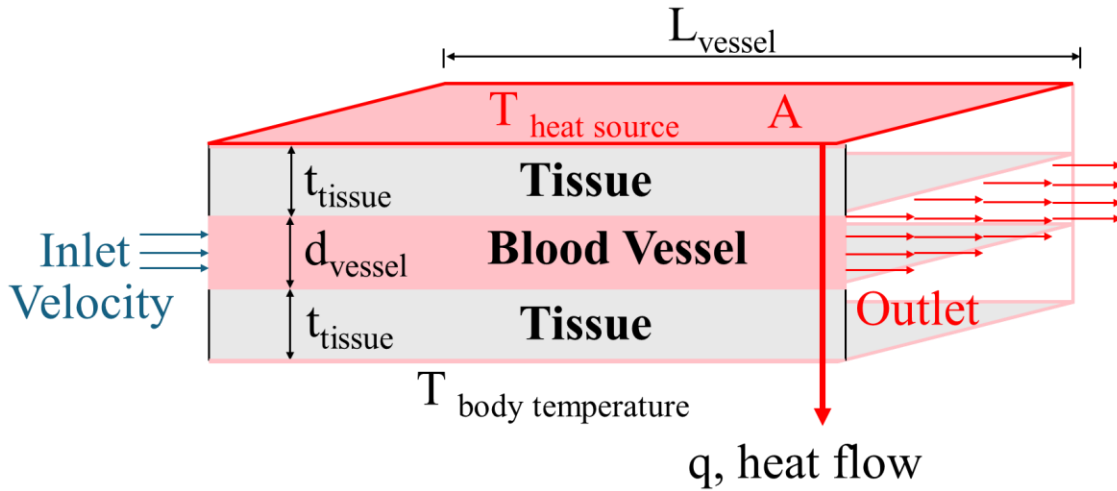


Figure 16: Heat Flow Schematic for 2D geometries, visualized by default as parallel plate in by Ansys Fluent computation

The conduction equation for the 2D case, after substitution of the appropriate variables is

$$\frac{q_{top\ wall}}{A} = \frac{k_{eff}(T_{heat\ source} - T_{body\ temperature})}{(t_{tissue} + t_{tissue} + d_{vessel})} \text{ (Eqn. 14 after 2D case substitution)}$$

This case accounts for the conduction across the full tissue composite. This implies that the “k” value within the equation is the effective thermal conductivity, k_{eff} . The overall concept of effective conductivity is applied in the human body as shown in Fig. 17.

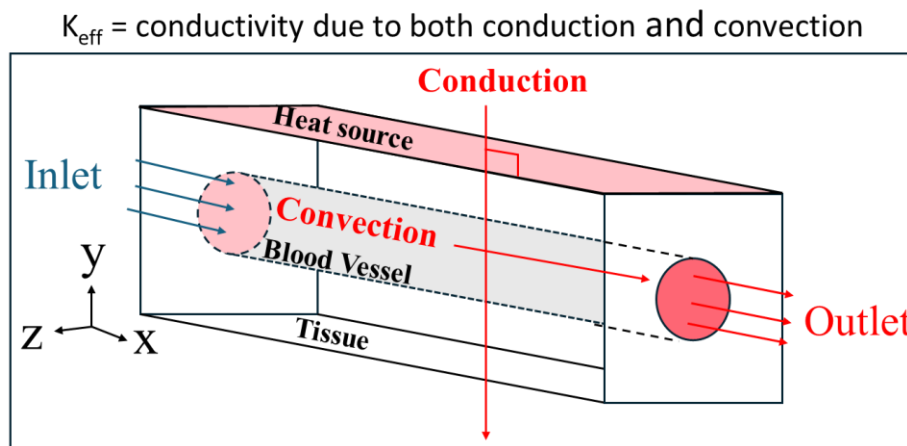


Figure 17: Visualization of Effective Thermal Conductivity in the Human Body

The impact of conduction through the tissue, and convection along the blood vessel are used to calculate effective conductivity in the 2D and 3D representations of this geometry.

The 3D temperature modeling was extended to validate the experimental outlet temperature using the temperature drop equations. The case was simplified in calculations such that the 3D pipe shown in the computational domain section was assigned a constant temperature condition of 333 K to make the case numerically solvable. The inlet temperature of the blood was known to be 311 K.

In the first case, the diameter was 2 mm, the length of the pipe was 15 cm, and the velocity was 10 cm/s. The second case used the same constant surface temperature condition of 333 K to analyze a different geometry with a 1 mm diameter, 15 cm length, and 5 cm/s velocity.

The equation for mass flow was defined as

$$\dot{m} = \rho VA \text{ (Eqn. 24)}$$

Additionally, the heat transfer coefficient, h , for pipe flow is found by using the formula for the Nusselt number,

$$Nu = \frac{\bar{h}D}{K} = 3.66 \text{ for a circular pipe (Eqn. 25)}$$

The results of Eqn. 24 and 25 are substituted into the equation for the temperature drop for a circular pipe with a constant surface temperature condition. The temperature at the outlet is calculated and verified using the temperature drop equation:

$$\frac{\Delta T_{m,o}}{\Delta T_{m,i}} = \frac{T_s - T_{m,o}}{T_s - T_{m,i}} = e^{\left(-\frac{PL}{\dot{m}c_p}\bar{h}\right)} \text{ (Eqn. 26)}$$

The outcomes of the calculation are shown in table 10 below.

Table 10: Temperature Drop Validation for 3D Geometry

Calculated Parameter	Case 1: D = 2 mm, V= 10 cm/s, L = 15 cm	Case 2: D = 1 mm, V = 5 cm/s, L =15 cm
Eqn. 24: $\dot{m} \left[\frac{g}{s}\right]$	0.32987	0.0412
Eqn. 25: $\bar{h} \left[\frac{W}{m^2K}\right]$	951.6	1903.2
Eqn. 26: $T_{m,o}$ [K]	322.625	332.946
Simulated (Ansys Fluent): $T_{m,o}$ [K] (Effect of Perfusion)	318.01	332.930
Temperature Difference between calculated and Ansys [K]	4.615	0.016

The agreement between the simulated and calculated results is very good. The outlet temperature in the simple constant temperature pressure drop calculation is slightly higher than the simulation. This is expected as the heat transfer through the computational geometry isn't a direct temperature drop condition in a pipe but rather considers the impact of perfusion and the overall tissue cross section as well. The results are also reasonable as the larger diameter case shows a higher temperature difference, showing that the results are scaling with anatomical size.

Impact of Fluid Viscosity on Simulation Results

Blood is a Non Newtonian Fluid and is commonly simulated via models that simulate its viscosity accordingly [36]. As discussed in the Ansys customization section, the Casson and Power Law models were used to simulate the impact of blood viscosity on the results using a user defined function. The results of this simulation were compared to the standard Newtonian model that is used in this experiment with a constant viscosity value of 4.5 m-Pas [57]. All cases had a 2 mm vessel diameter, 15 mm length, and 10 cm/s velocity.

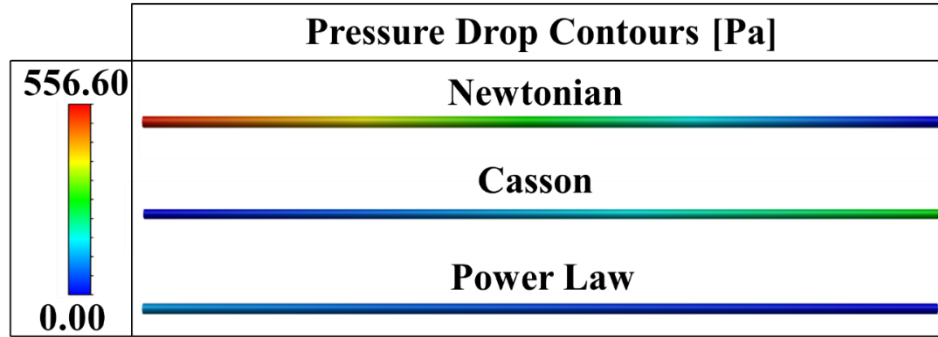


Figure 18: Pressure Drop within the Blood Vessel Embedded in the Computational Geometry for the Models comparing Newtonian and Non-Newtonian Flow

As seen in Fig. 18, the pressure drop from one end of the vessel to the other is most pronounced in the Newtonian model. It decreases with the Casson model and further with the Power Law model. This result implies that the validation methods used in this result for fluid properties would change if Non Newtonian models were to be used. This is one reason that the model was simplified, and a constant viscosity value was used.

Additionally, the thermal results were compared. There was no change in the heat transfer profile that was generated for both the full tissue composite and within the vessel itself. The Newtonian model is sufficient for the purpose of this study as the primary output of the study, effective thermal conductivity, will remain the same as this thermal output. Figs. 19 and 20 show the temperature contours for these simulations, with no difference in the contours and temperature ranges between the Newtonian, Casson, and Power Law model.

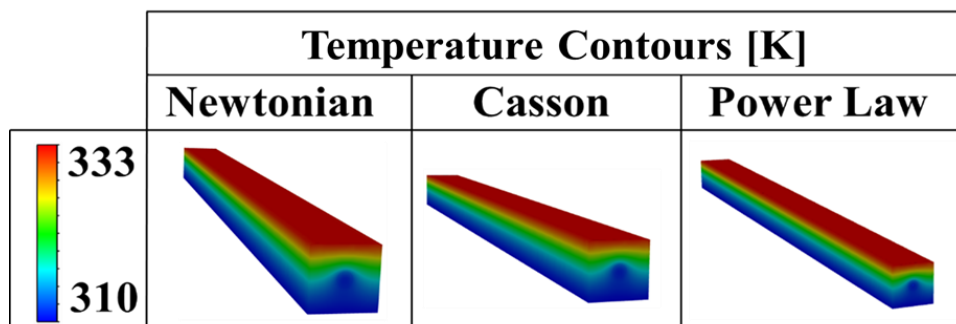


Figure 19: Temperature Contours of the Computational Domains Comparing Newtonian and Non-Newtonian Flow Models

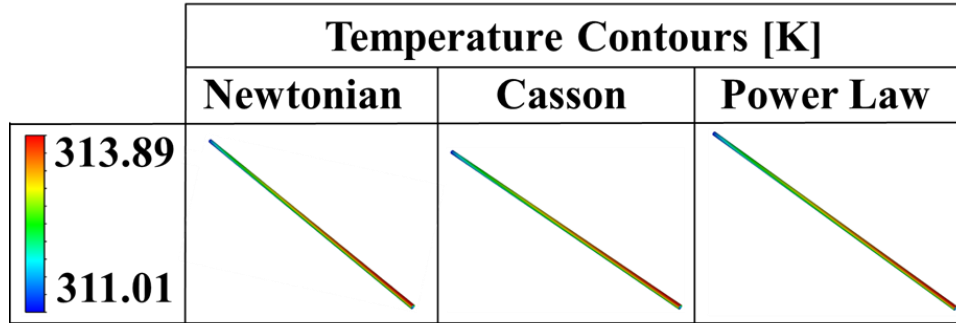


Figure 20: Temperature Contour the Blood Vessel Embedded in the Computational Domain, Comparing Newtonian and Non-Newtonian Flow Models

The geometry shown within Fig. 20 is the contour of the embedded vessel which was extracted from the tissue to analyze the internal flow effects. The inlet temperature is 311.01 K, and the outlet temperature is 313.89 K for the Newtonian model and 313.79 K for the Casson and Power Law models. Additionally, the temperature drop across the vessel follows the same visual pattern, where the fluid heats up rapidly with blood flow, proving that the Newtonian, Casson, and Power Law models have little impact on the results of this experiment. Therefore, the use of the Newtonian viscosity model is appropriate as it remains accurate while decreasing computational time of the CFD simulations.

Effect of Top Wall Temperature on Varying Applications

The impact of the top wall temperature on the effective thermal conductivity was assessed. The top wall boundary of 333 K was used for the parametric studies in this experiment (typically seen in radiotherapy, surgery, and ablation applications [1] [57]). The temperature chosen has a large enough difference between the higher and lower temperatures which makes it easier to visualize the contours. Another experiment was conducted with a top wall temperature of 313 K that is more indicative of a breast cancer heat source with a bottom wall healthy tissue temperature of 306 K. These values were based on Gautherie's in vivo measurements of cancerous and healthy tissues [5].

The effective thermal conductivity was calculated for the high and low temperature cases using Eqn. 14. The results of the two cases are given below in Fig. 21. Both cases shown have a 2 mm vessel diameter, 15 mm length, and 10 cm/s flow velocity. The low temperature case was used to validate the results of the effective thermal conductivity measurements conducted by Gautherie.

The tissue properties discussed in the methods section were based on the soft tissue found in the average fatty human breast as documented by S. Camilleri et. al. and can be used for this comparison [57].

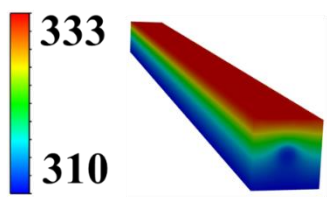
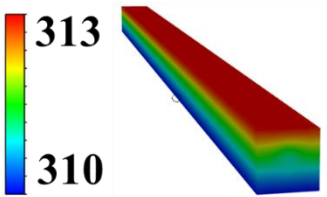
	High Heat (333 K)	Low Heat (313 K)
Temperature Contour [K]		
K_{eff}	4.06 mW/cm-K	2.97 mW/cm-K
Use Cases	Ablation surgery Surface burns	Cancer Rapid Angiogenesis

Figure 21: Impact of Top Wall Temperature on Effective Thermal Conductivity of fatty tissue and the Use Cases of the Wall Temperatures

The results show that effective thermal conductivity varies with the boundary temperature. The temperature contours follow the same pattern for both cases, but the difference in temperature is much less pronounced between layers at a lower temperature.

By extension, this result implies that the application of this bioheat transfer experiment can be used in any heat transfer output including a cancer heat source, surgical application of heat or cold, or other surface heating applications of tissue so long as the tissue doesn't experience any significant structural or material deformation and follows the laws of conservation of energy and mass. Other combinations of temperature sources are possible and will require customization for the application.

The effective thermal conductivity was verified with Gautherie's measurements that Gutierrez extracted for cancerous breast tissue. The mean effective thermal conductivity of cancerous breast tissue was measured to be 2.80 mW/cm-K in vitro and 5.11 mW/cm-K in vivo. Likewise for healthy tissue, based on the fat, fibrous, and glandular composition, the conductivity lies between 1.20 mW/cm-K and 3.70 mW/cm-K. An increased fat content implies lower

conductivity within this range, whereas glandular tissue has the highest conductivity in healthy specimens [61] [56] .

Based on this information, the true value of perfused tissue with a cancerous boundary is expected to lie between cancerous and healthy tissue. The cases that were simulated with one well defined vessel use data from fatty soft tissue. Their effective conductivity was simulated to be 2.97 mW/cm-K (Fig. 21). This outcome is reasonable as the thermal conductivity remains significantly higher than the fatty healthy tissue and is within the cancerous range. Diving further into the numbers, the conductivity of normal fatty tissue is approximately close to 1.20 mW/cmK as described by Gutierrez. The result of the above is not only within the cancerous range, but is significantly elevated, showing the impact of well-defined vascularization under heat stress.

Gutierrez further analyzed and extracted Gautherie's data comparing the temperature of the measured temperature to effective thermal conductivity. Fig. 22 a shows that the presence of the tumor increased conductivity in comparison to a healthy breast, and graphs the relationship between the two for each measurement [61] [56]. The tissue with a top wall boundary of 313 K (40 °C) has a slightly higher temperature than that provided above. The value was chosen as a benchmark that remains above the human body core temperature (310 K) that is the bottom boundary of the computational geometry. Further experimentation is needed for the lower temperatures measured in breast tissues, and for the various compositional characteristics (fatty, fibrous, and glandular) measured in past experiments. The conductivity value of 2.97 mW/cm-K is predicted to be lower than Fig. 22 a as the current cross section doesn't include the fibroglandular elements of the tissue. Looking further into Fig. 22 b, the value aligns with the conductivity of early stage cancer (k_{eff} line 1) where the probe reaches the center of the cancer at 25 mm. This cancer would have a low level of vascularization which is typical of early stage cancers, further validating the results of this one vessel experiment.

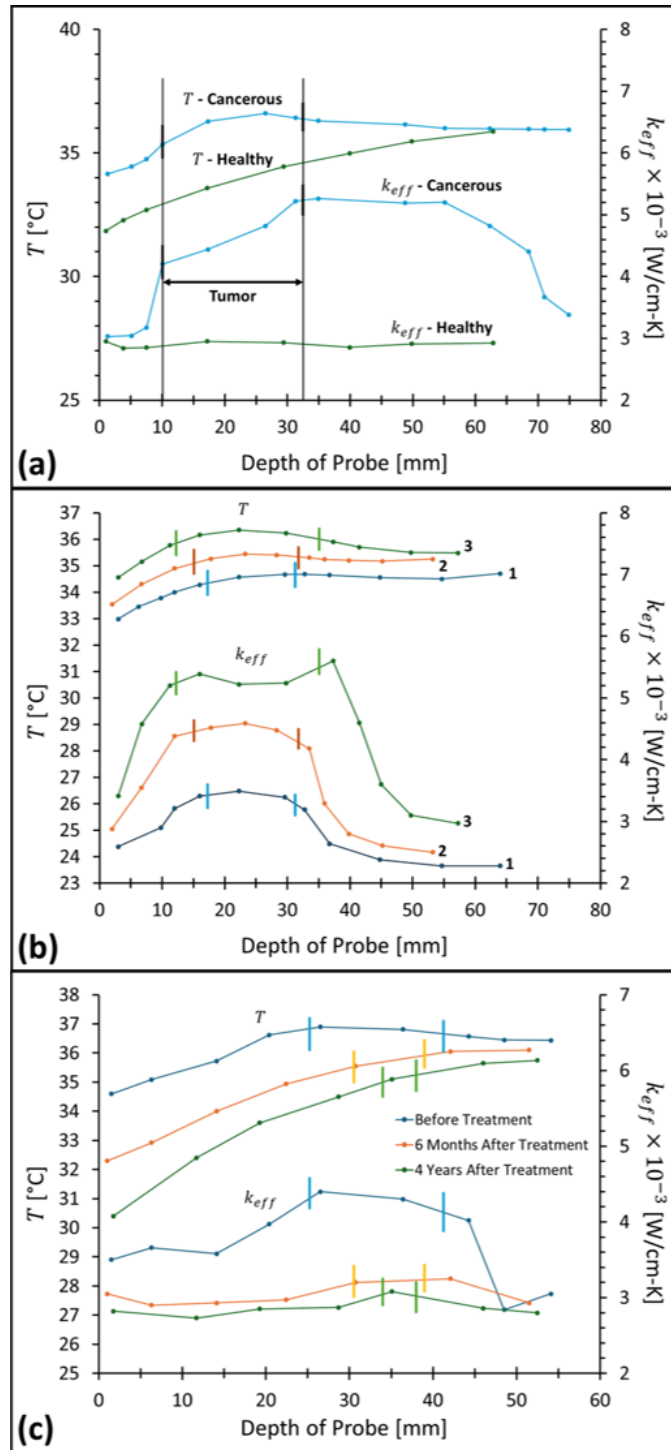


Figure 22: Measured temperatures and effective thermal conductivity, a) comparing a healthy and cancerous breast using measurements b) depicting cancer progression over time and c) showing change with treatment from Gautherie and recreated by Gutierrez [61] [56]

6.2 Outcomes of the 2D Parametric Simulations

The results of the verification and validation indicate that the expected theory matched the given. Therefore, the parametric study was conducted using the base setup given in Fig. 12. The parameters analyzed were the diameter of the vessel, velocity of blood flow, and the length of the vessel as given in Fig. 23, 24, and 25. These variables were modified one at a time for four categories of vasculature. These are the capillaries, arterioles, medium sized arteries, and artery branches in order of increasing size. Each parameter that was held constant was ensured to fit the average values for the category of vasculature that was being assessed. The output variable of interest was the heat flux of the system which was used to derive effective thermal conductivity as shown in Eqn. 14.

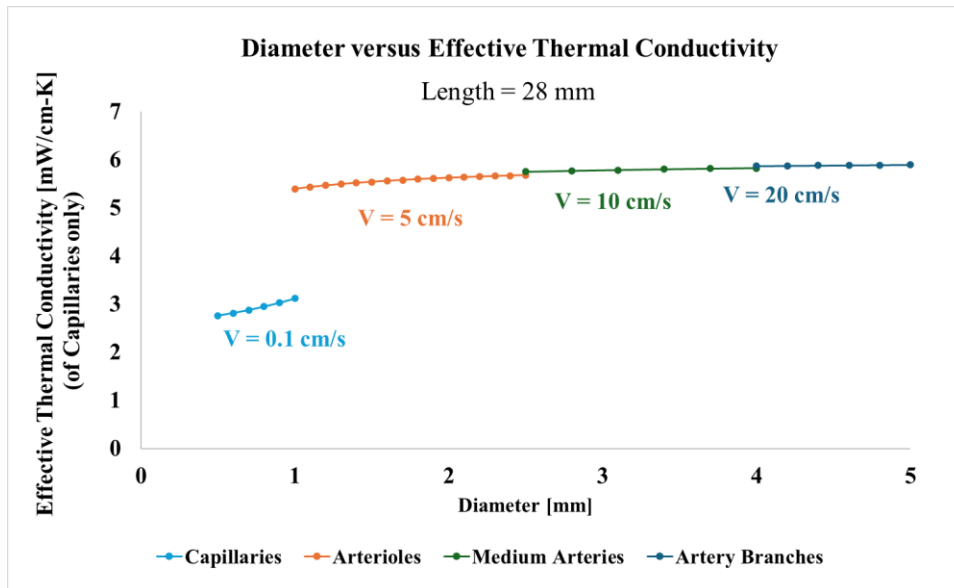


Figure 23: Diameter versus Effective Thermal Conductivity 2D Parametric Study

The diameter causes a rapid increase in effective thermal conductivity in capillaries as the increase of surface area of the vessel to the size of the tissue is very large (Fig. 23). This result is expected as capillaries provide significantly impact cellular level processes due to the contact with the tissues [16]. They serve as important factors in oxygenation of tissues and are labeled the most thermally significant in addition to their primary responsibility of providing blood flow [12]. The impact of the diameter tapers off quickly as seen by the arterioles, medium sized arteries, and artery branches graphed on the secondary axis.

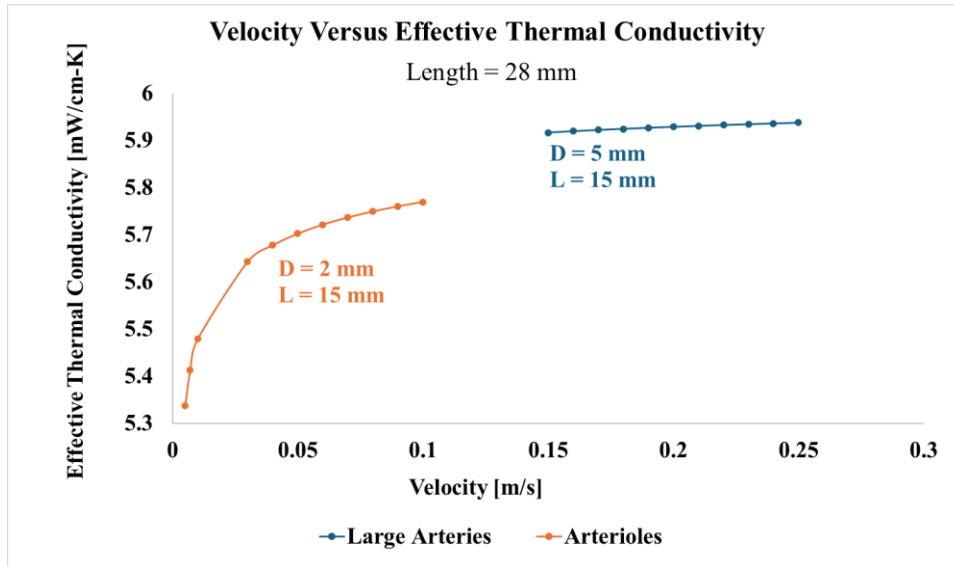


Figure 24: Velocity versus Effective Thermal Conductivity 2D Parametric Study

The impact of velocity was simulated for arterioles and large vessels (Fig. 24). As seen, the arteriole sized vasculature is expected to have a larger variance in effective conductivity than that of the large artery. There is a 0.5 mW/cm-K variance for arterioles, whereas this decreases to less than 0.05 mW/cm-K over the same velocity range in larger arteries. The trend of smaller arteries having more thermal significance continues. The ranges of velocities chosen were those that are anatomically normal, as given in Table 2.

Lastly, Fig. 25 shows the results of varying the length of the computational geometry. The length has a significant impact in the first part of the curve at first and then tapers off into a constant value. This effect could be due to the initial entrance effects in the simulation and has scope for further investigation. A derivation is needed to calculate the thermal entrance length of this 2D flow for this assessment (represented by default in Ansys as a parallel plate problem given in Fig. 16).

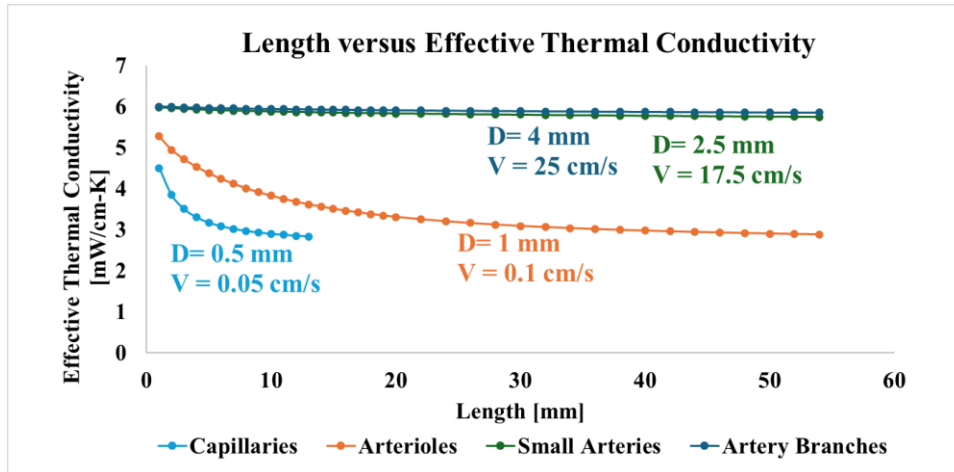


Figure 25: Length versus Effective Thermal Conductivity 2D Parametric Study

6.3 Outcomes of the 3D Parametric Simulations

The simulated values for the 3D parametric results are given below. The diameter, velocity, and length of the computational geometry given in Fig. 13 was varied according to the values in Table 2, while varying only one parameter at a time. The effective thermal conductivity was calculated using the heat flux output from Ansys and Eqn. 14. Varying the diameter yielded similar results to the 2D parametric outcomes, where the capillaries have a huge thermal impact within their range. The larger sized capillaries (closer to 1 mm diameter) have increasing heat transfer with conductivity increasing by 0.4 mW/cm-K within a 0.5 mm increase in diameter. Arterioles above 1 mm, while having higher conductivity overall, do not have such a large increase. The conductivity increases approximately by 1 mW/cm-K over 1.5 mm and tapers off with increasing diameter. The results align with the findings that capillaries are the most thermally significant vessels [12]. Capillaries are also the first to develop in the process of angiogenesis, as the typical blood vessel generation process includes branching from existing ends to have the same or smaller diameter at first, and then pruning increases the size of the vessel based on the bodily need, and as the vessel increases in length [23]. The outcome shows why cancers with angiogenesis in tissues have such a high thermal impact.

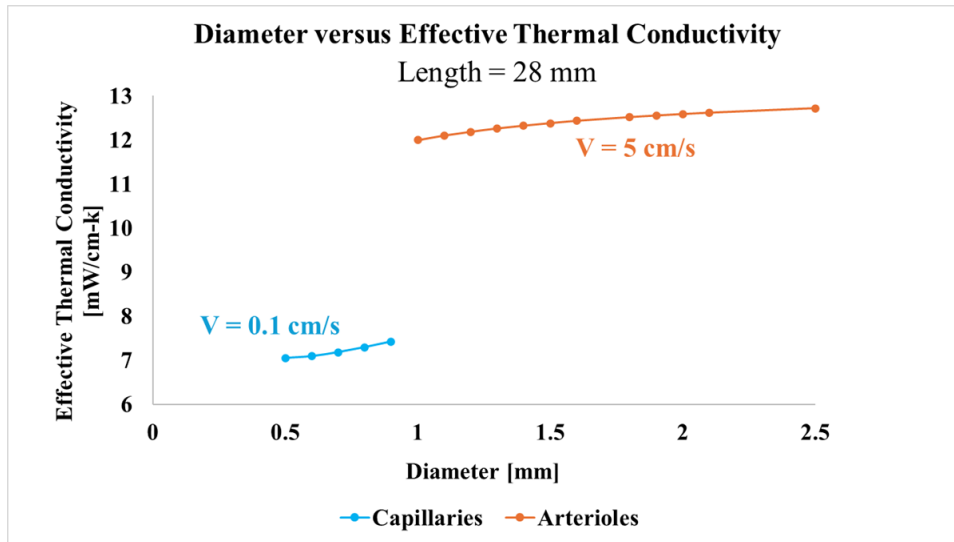


Figure 26: Diameter versus Effective Thermal Conductivity 3D Parametric Study

The patterns found by varying the velocity over and length also align with the 2D study. Once again, Fig. 27 the smaller arterioles have a larger variation in effective conductivity as velocity changes. The artery branches are presented on the secondary axis and show very little increase (0.3 mW/cm-K) in conductivity with velocity in comparison to the smaller vessels which have a large jump within their respective velocity ranges. Length causes a decrease in conductivity at first (Fig. 28), and then tapers off after the first part of the curve. Then, the effective conductivity remains constant. Similar patterns are seen for vessels larger than capillaries, but the full taper is not visible within the lengths selected.

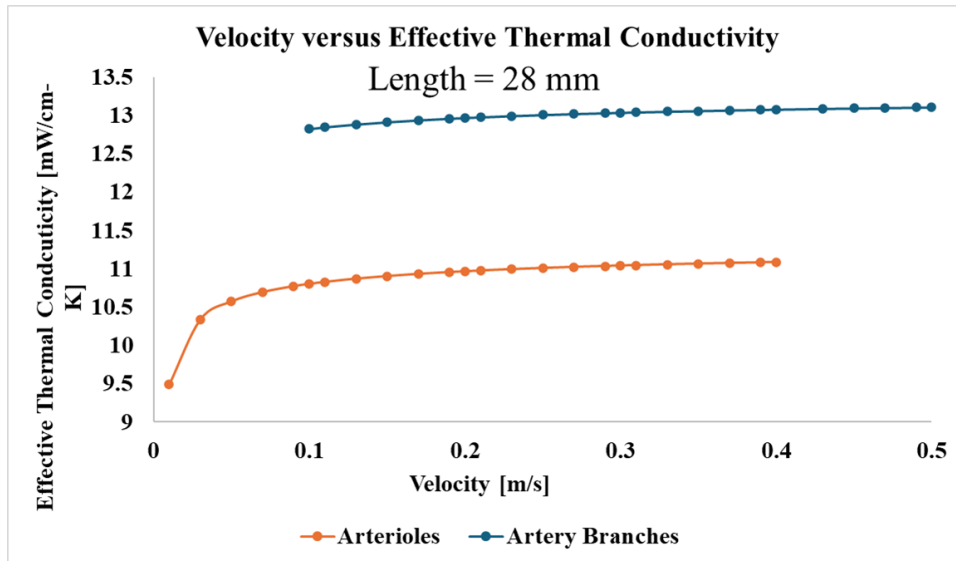


Figure 27: Velocity versus Effective Thermal Conductivity 3D Parametric Study

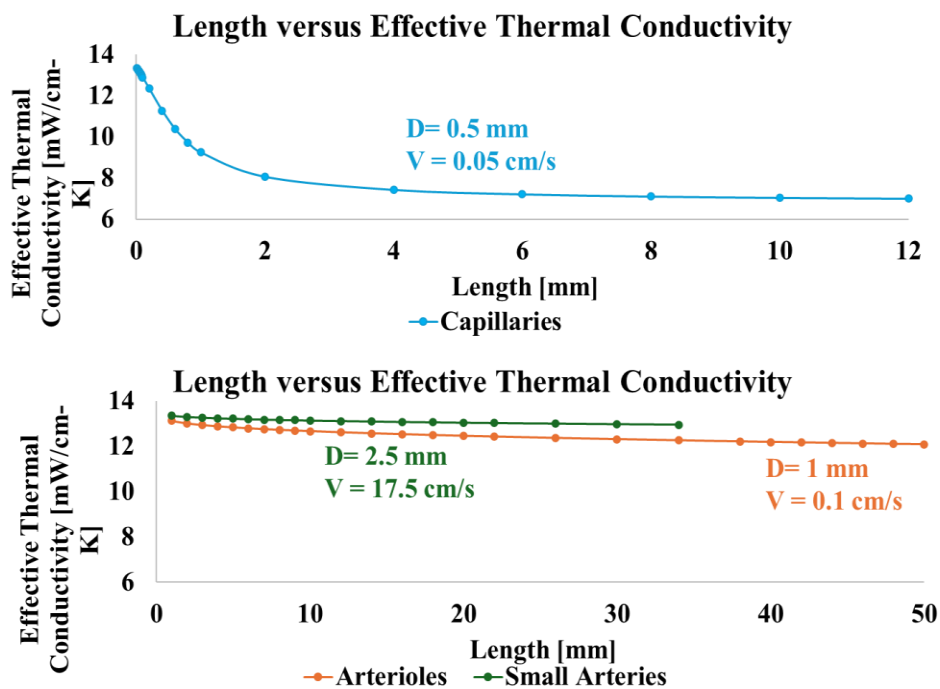


Figure 28: Length versus Effective Thermal Conductivity 3D Parametric Study

6.4 The Impact of Multivessel Flow on Effective Thermal Conductivity

Three different vessel configurations were tested in addition to the single vessel flow to assess the impact of having multiple vessels and their orientation. While vasculature is not as neatly stacked as shown, these results explain what conditions have the most impact.

The setup was conducted by taking the same tissue cross section geometry used throughout this experiment and copying it beside each other. The boundary between the old and new vessel was melded together with a share topology function and zero contact resistance to simulate one cohesive tissue cross section with the vessels embedded. The vessels were tested with two vessels in a row, two vessels in a column, and four vessels making a two row and two column matrix. The results were compared to the effective thermal conductivity of one vessel.

The conductivity of the tissue does not change when the vessels are placed beside each other. This result is reasonable as the distribution of heat flow is vertical throughout the tissue and so the flow of heat is the same. In contrast, the conductivity of the tissue approximately doubles when a second row of vessels is added. The resulting effective thermal conductivity values are given in Fig. 29.

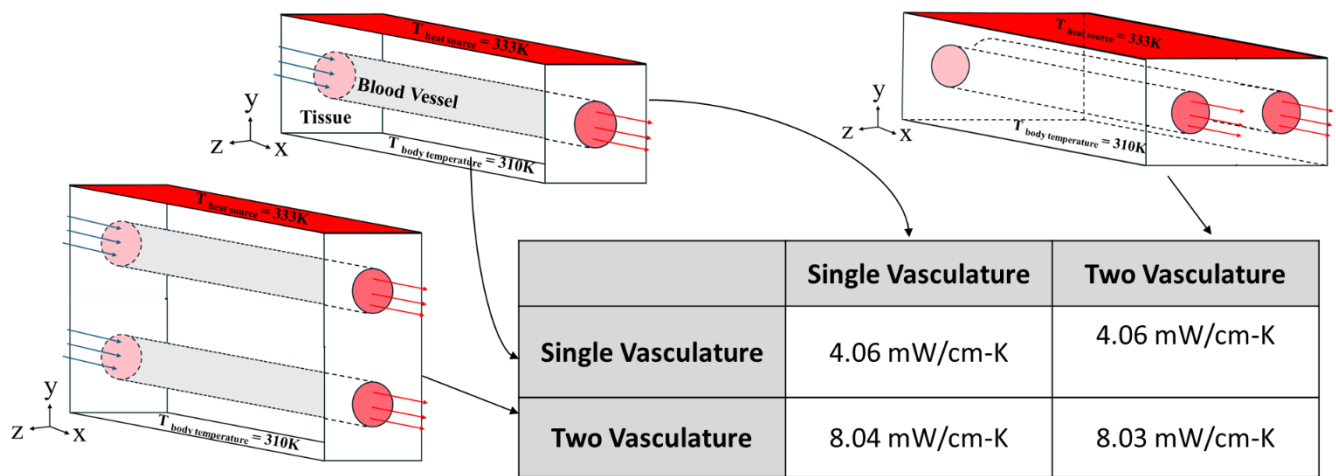


Figure 29: Effective Thermal Conductivity and contour comparison of multivessel flow configurations

The analysis is a preliminary extension of the research above and is an illustration of future work that is needed to establish the impact of effective thermal conductivity in multivessel flows. Other factors such as vessel spacing, orientation, and the impact of branching can be considered in more detail for this topic.

6.5 Use of Effective Thermal Conductivity as a Substitute to Vasculature

While the effective thermal conductivity has been calculated, the question remains if it can be used as a substitute for a tissue. Fig. 30 below shows the difference between the solid tissue

temperature contours of the solid tissue without vasculature and the same effective conductivity (4.7 mW/cm-K) as the tissue with embedded vasculature given on the right. It is obvious while comparing the two top images that the flow of heat throughout the tissues is quite similar. It follows a top down pattern with a gradient that evens out as it goes farther from the tissue. Therefore, effective thermal conductivity can be used as a substitute for the blood vessel model if the full tissue needs to be analyzed in the context of heat transfer.

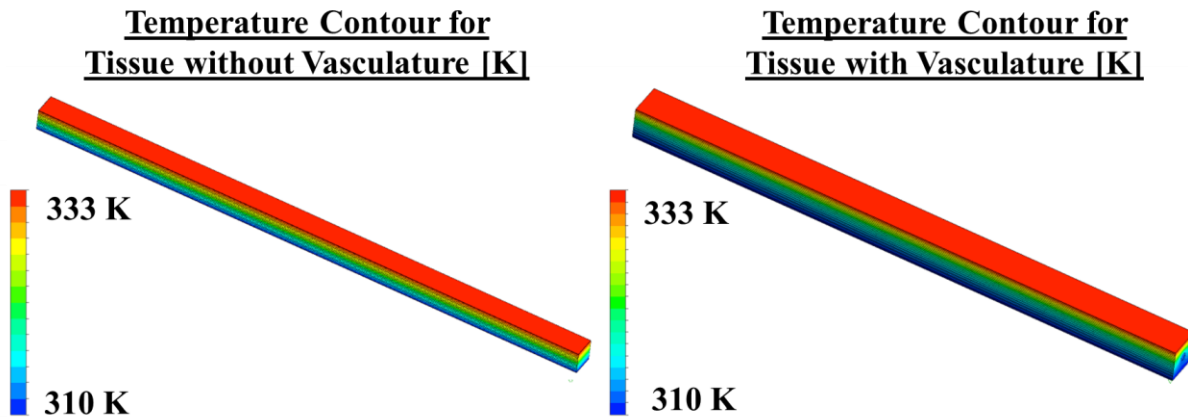


Figure 30: Temperature Contours of Solid Tissue without Vasculature and Tissue with an Embedded Vessel

7.0 CONCLUSION

The objectives of the work were to understand the impact of vasculature on effective thermal conductivity, k_{eff} , of a tissue cross section. The task was broken down to simulate the effect of vessel length, diameter, and flow velocity in 2D and 3D regimes using CFD. The simulations were conducted using anatomically valid data and key assumptions including steady state laminar flow, the presence of a uniform blood vessel cross section, and a Newtonian fluid assumption for blood. The validation of the results was conducted using pressure drop and temperature drop equations for the fundamental theory. The effective thermal conductivity measurements were validated using Gautherie's research. The use of the Newtonian properties of blood versus Non-Newtonian models was tested. Additionally, the impact of the top wall temperature and multiple vessels in the tissue were assessed for their relevance.

The results were that diameter impacts k_{eff} in a nonlinear manner. The capillaries have the most impact and the largest capillaries are the most thermally significant. The impact of velocity on tissue conductivity was positive and nonlinear. An increase in length led to conductivity tapering off to a constant after an initial decrease. In each case, the jumps in the curves indicated that conductivity transitions rapidly between capillaries, arterioles, medium arteries, and artery branches. The 2D and 3D results matched in patterns, even though the geometrical differences between the flows prevented them from reaching the same numerical values of temperature and pressure drop. Additionally, Newtonian flow was shown to be sufficient for this model as the Casson and Power Law models which are analyzed did not have any major thermal impact.

The results were validated using Gautherie's effective thermal conductivity measurements at a lower temperature than the parametric simulations, showing that the effective conductivity is valid for several temperatures. The multiple vessel flow analysis revealed that stacking vessels vertically had more impact on conductivity than spreading them out horizontally against a heat source.

This research has several applications. First, it adds to the fundamental bioheat transfer theory by analyzing the impact of blood vessel geometry and orientation. It tackles some questions that remained unknown with traditional bioheat transfer mathematical models. Second, it analyzes a high and low heat transfer case and shows the relevance of effective thermal conductivity as it applies to both damaging heat sources, and lower temperatures such as cancer. This parameter is

versatile and can be used in conjunction with any heat transfer source in tissues. Lastly, effective thermal conductivity can be used as a substitute for blood vessels when simplification is possible. This was proven by a comparative analysis of a tissue with the blood vessel removed and the same conductivity as a tissue with the original parameters and an embedded blood vessel.

8.0 LIMITATIONS AND FUTURE WORK

The research into the effective thermal conductivity of live tissues is only a starting point and leaves significant room for future work. The first limitation of the research is that the 2D models required further derivation of the temperature drop and were different from the 3D models in their fundamental structure. This leaves scope for development of the theory. The difference between the two models can be assessed to understand if saving computational time is helpful.

Second, the materials were limited in selection to focus on the derivation of patterns. Further cases can be analyzed to see if the tissues respond differently. For instance, fibrous and glandular sections can be analyzed in more detail for breast cancer.

Additional patterns for vessel configuration need to be considered. These include the branching structure of vessels, the spacing between vessels, less defined or leakier vasculature in angiogenesis, and cardiac tissue. There are several angiogenic dependent processes such as kidney cancer, retinal cancer, and embryogenesis [20] which can be interesting to analyzed in the context of the thermal properties they possess for their vascularity. Other angiogenesis phenomena that could be considered include interstitial flows and porosity. Lastly the deformation of tissues due to surgery and heat transfer can be considered further at higher temperatures.

9.0 SOCIETAL CONTEXT

Heat transfer is a highly relevant subject within the human body. It has been studied extensively in applications such as thermal scanning, core body temperature regulation, and for differentiating properties of normal and abnormal tissues. Treatment processes such as cryosurgery and ablation are commonly used for several cancers, malignant masses, and within heart tissues. This subject is also applicable while understanding how the body's thermal signature changes with the development of blood vessels due to phenomena such as normal tissue growth or cancer growth.

Tissue modeling has been instrumental in comprehending interactions within the human body. The advent of advanced computing power, combined with research on biochemical reactions within live tissues, has led to the development of increasingly accurate models. One important application of such modeling is within breast cancer, which consists of over 30% of cases within female cancers and affects around 300,000 women yearly [66]. Another application is the use of heat transfer to conduct minimally invasive surgery with increasing accuracy [1]. The research presented within this paper is an effort to study how tissues function via computer modeling to contribute to the field of bioheat transfer which is applied in both engineering and medicine.

10.0 REFERENCES

- [1] Shrivastava, D., ed., 2018, *Theory and Applications of Heat Transfer in Humans*, Wiley, Hoboken, NJ.
- [2] Etehadtavakol, M., and Ng, E. Y. K., 2020, “Survey of Numerical Bioheat Transfer Modelling for Accurate Skin Surface Measurements,” *Thermal Science and Engineering Progress*, **20**, p. 100681.
- [3] Hristov, J., 2019, “Bio-Heat Models Revisited: Concepts, Derivations, Nondimensionalization and Fractionalization Approaches,” *Front. Phys.*, **7**, p. 189.
- [4] D’Alessandro, G., Tavakolian, P., and Sfarra, S., 2024, “A Review of Techniques and Bio-Heat Transfer Models Supporting Infrared Thermal Imaging for Diagnosis of Malignancy,” *Applied Sciences*, **14**(4), p. 1603.
- [5] Gautherie, M., 1980, “THERMOPATHOLOGY OF BREAST CANCER: MEASUREMENT AND ANALYSIS OF IN VIVO TEMPERATURE AND BLOOD FLOW,” *Ann NY Acad Sci*, **335**(1 Thermal Chara), pp. 383–415.
- [6] Gautherie, M., and Gros, C. M., 2006, “Breast Thermography and Cancer Risk Prediction,” *Cancer*, **45**(1), pp. 51–56.
- [7] Rubenstein, D. A., Yin, W., and Frame, M. D., 2022, *Biofluid Mechanics: An Introduction to Fluid Mechanics, Macrocirculation, and Microcirculation*, Academic Press, an imprint of Elsevier, London, United Kingdom ; San Diego, CA.
- [8] Griffioen, A. W., 2011, “Angiogenesis,” *Encyclopedia of Cancer*, M. Schwab, ed., Springer Berlin Heidelberg, Berlin, Heidelberg, pp. 185–186.
- [9] Charny, C. K., 1992, “Mathematical Models of Bioheat Transfer,” *Advances in Heat Transfer*, Elsevier, pp. 19–155.
- [10] Weinbaum, S., and Jiji, L. M., 1985, “A New Simplified Bioheat Equation for the Effect of Blood Flow on Local Average Tissue Temperature,” *Journal of Biomechanical Engineering*, **107**(2), pp. 131–139.

- [11] Valvano, J. W., 2006, "Bioheat Transfer," *Encyclopedia of Medical Devices and Instrumentation*, J.G. Webster, ed., Wiley.
- [12] 2000, *The Biomedical Engineering Handbook. 2*, CRC Press, Boca Raton, Fla.
- [13] Chato, J. C., 1980, "Heat Transfer to Blood Vessels," *Journal of Biomechanical Engineering*, **102**(2), pp. 110–118.
- [14] Chen, M. M., and Holmes, K. R., 1980, "MICROVASCULAR CONTRIBUTIONS IN TISSUE HEAT TRANSFER," *Annals of the New York Academy of Sciences*, **335**(1), pp. 137–150.
- [15] Chung, K. W., and Chung, H. M., 2012, *Gross Anatomy*, Wolters Kluwer/Lippincott, Williams & Wilkins, Philadelphia, Pa.; London.
- [16] J. Gordon Betts, Kelly A. Young, James A. Wise, Eddie Johnson, Brandon Poe, Dean H. Kruse, Oksana Korol, Jody E. Johnson, Mark Womble, and Peter DeSaix, 2013, *Anatomy and Physiology*, OpenStax, Houston, Texas.
- [17] Julià-Sapé, M., Candiota, A. P., and Arús, C., 2019, "Cancer Metabolism in a Snapshot: MRS(I)," *NMR in Biomedicine*, **32**(10).
- [18] Costanzo, L. S., 2018, *Physiology*.
- [19] Folkman, J., 1997, "Angiogenesis and Angiogenesis Inhibition: An Overview," *Regulation of Angiogenesis*, I.D. Goldberg, and E.M. Rosen, eds., Birkhäuser Basel, Basel, pp. 1–8.
- [20] Folkman, J., 2001, "Angiogenesis-Dependent Diseases," *Seminars in Oncology*, **28**(6), pp. 536–542.
- [21] Ellis, L. M., and Fidler, I. J., 1996, "Angiogenesis and Metastasis," *European Journal of Cancer*, **32**(14), pp. 2451–2460.
- [22] Kothari, C., Diorio, C., and Durocher, F., 2020, "The Importance of Breast Adipose Tissue in Breast Cancer," *IJMS*, **21**(16), p. 5760.

- [23] Folkman, J., 2002, "Role of Angiogenesis in Tumor Growth and Metastasis," *Seminars in Oncology*, **29**(6), pp. 15–18.
- [24] Rieger, H., Fredrich, T., and Welter, M., 2016, "Physics of the Tumor Vasculature: Theory and Experiment," *Eur. Phys. J. Plus*, **131**(2), p. 31.
- [25] Koumoutsakos, P., Pivkin, I., and Milde, F., 2013, "The Fluid Mechanics of Cancer and Its Therapy," *Annu. Rev. Fluid Mech.*, **45**(1), pp. 325–355.
- [26] Cao, Y., Arbiser, J., D'Amato, R. J., D'Amore, P. A., Ingber, D. E., Kerbel, R., Klagsbrun, M., Lim, S., Moses, M. A., Zetter, B., Dvorak, H., and Langer, R., 2011, "Forty-Year Journey of Angiogenesis Translational Research," *Science Translational Medicine*, **3**(114), pp. 114rv3-114rv3.
- [27] Shchors, K., and Evan, G., 2007, "Tumor Angiogenesis: Cause or Consequence of Cancer?," *Cancer Research*, **67**(15), pp. 7059–7061.
- [28] Folkman, J., 1975, "Tumor Angiogenesis: A Possible Control Point in Tumor Growth," *Ann Intern Med*, **82**(1), p. 96.
- [29] Liao, D., and Johnson, R. S., 2007, "Hypoxia: A Key Regulator of Angiogenesis in Cancer," *Cancer Metastasis Rev*, **26**(2), pp. 281–290.
- [30] Santisteban, G. A., Ely, J. T. A., Hamel, E. E., Read, D. H., and Kozawa, S. M., 1985, "Glycemic Modulation of Tumor Tolerance in a Mouse Model of Breast Cancer," *Biochemical and Biophysical Research Communications*, **132**(3), pp. 1174–1179.
- [31] Giannokostas, K., Dimakopoulos, Y., and Tsamopoulos, J., 2022, "Shear Stress and Intravascular Pressure Effects on Vascular Dynamics: Two-Phase Blood Flow in Elastic Microvessels Accounting for the Passive Stresses," *Biomech Model Mechanobiol*, **21**(6), pp. 1659–1684.
- [32] Campinho, P., Vilfan, A., and Vermot, J., 2020, "Blood Flow Forces in Shaping the Vascular System: A Focus on Endothelial Cell Behavior," *Front. Physiol.*, **11**, p. 552.

- [33] Roux, E., Bougaran, P., Dufourcq, P., and Couffinhal, T., 2020, “Fluid Shear Stress Sensing by the Endothelial Layer,” *Front. Physiol.*, **11**, p. 861.
- [34] Jackson, T. L., ed., 2012, *Modeling Tumor Vasculature: Molecular, Cellular, and Tissue Level Aspects and Implications*, Springer, New York.
- [35] Secomb, T. W., 2016, “Hemodynamics,” *Compr Physiol*, **6**(2), pp. 975–1003.
- [36] Husain, I., Labropulu, F., Langdon, C., and Schwark, J., 2013, “A Comparison of Newtonian and Non-Newtonian Models for Pulsatile Blood Flow Simulations,” *Journal of the Mechanical Behaviour of Materials*, **21**(5–6), pp. 147–153.
- [37] Truskey, G. A., Yuan, F., and Katz, D. F., 2009, *Transport Phenomena in Biological Systems*, Pearson Prentice Hall, Upper Saddle River, N.J.
- [38] Mada, J., and Tokihiro, T., 2022, “Pattern Formation of Vascular Network in a Mathematical Model of Angiogenesis,” *Japan J. Indust. Appl. Math.*, **39**(1), pp. 351–384.
- [39] Talou, G. D. M., Safaei, S., Hunter, P. J., and Blanco, P. J., 2021, “Adaptive Constrained Constructive Optimisation for Complex Vascularisation Processes,” *Sci Rep*, **11**(1), p. 6180.
- [40] Qohar, U. N. A., Munthe-Kaas, A. Z., Nordbotten, J. M., and Hanson, E. A., 2020, *A Multi-Scale Flow Model for Blood Regulation in a Realistic Vascular System*, In Review.
- [41] Coccarelli, A., Carson, J. M., Aggarwal, A., and Pant, S., 2021, “A Framework for Incorporating 3D Hyperelastic Vascular Wall Models in 1D Blood Flow Simulations,” *Biomech Model Mechanobiol*, **20**(4), pp. 1231–1249.
- [42] Senarathna, J., Prasad, A., Bhargava, A., Gil, S., Thakor, N. V., and Pathak, A. P., 2020, “HemoSYS: A Toolkit for Image-Based Systems Biology of Tumor Hemodynamics,” *Sci Rep*, **10**(1), p. 2372.
- [43] Wu, C., Hormuth, D. A., Oliver, T. A., Pineda, F., Lorenzo, G., Karczmar, G. S., Moser, R. D., and Yankeelov, T. E., 2020, “Patient-Specific Characterization of Breast Cancer Hemodynamics Using Image-Guided Computational Fluid Dynamics,” *IEEE Trans. Med. Imaging*, **39**(9), pp. 2760–2771.

- [44] Kamada, H., Nakamura, M., Ota, H., Higuchi, S., and Takase, K., 2022, “Blood Flow Analysis with Computational Fluid Dynamics and 4D-Flow MRI for Vascular Diseases,” *Journal of Cardiology*, **80**(5), pp. 386–396.
- [45] Yogeswaran, S., and Liu, F., 2021, *Vascular Flow Simulations Using SimVascular and OpenFOAM*, Cardiovascular Medicine.
- [46] Moath, A., Xu Xiao, Y., and Department of Chemical Engineering Imperial College London, South Kensington Campus, London, United Kingdom, 2021, “The Influence of Tumour Vasculature on Fluid Flow in Solid Tumours: A Mathematical Modelling Study,” *Biophysics Reports*, **7**(1), pp. 35–54.
- [47] Zudaire, E., Gambardella, L., Kurcz, C., and Vermeren, S., 2011, “A Computational Tool for Quantitative Analysis of Vascular Networks,” *PLoS ONE*, **6**(11), p. e27385.
- [48] Haft-Javaherian, M., Fang, L., Muse, V., Schaffer, C. B., Nishimura, N., and Sabuncu, M. R., 2019, “Deep Convolutional Neural Networks for Segmenting 3D in Vivo Multiphoton Images of Vasculature in Alzheimer Disease Mouse Models,” *PLoS ONE*, **14**(3), p. e0213539.
- [49] Bumgarner, J. R., and Nelson, R. J., 2022, “Open-Source Analysis and Visualization of Segmented Vasculature Datasets with VesselVio,” *Cell Reports Methods*, **2**(4), p. 100189.
- [50] Shen, J., Faruqi, A. H., Jiang, Y., and Maftoon, N., 2021, “Mathematical Reconstruction of Patient-Specific Vascular Networks Based on Clinical Images and Global Optimization,” *IEEE Access*, **9**, pp. 20648–20661.
- [51] Cury, L. F. M., Maso Talou, G. D., Younes-Ibrahim, M., and Blanco, P. J., 2021, “Parallel Generation of Extensive Vascular Networks with Application to an Archetypal Human Kidney Model,” *R. Soc. open sci.*, **8**(12), p. 210973.
- [52] Jia, D., and Zhuang, X., 2021, “Learning-Based Algorithms for Vessel Tracking: A Review,” *Computerized Medical Imaging and Graphics*, **89**, p. 101840.
- [53] Metzcar, J., Wang, Y., Heiland, R., and Macklin, P., 2019, “A Review of Cell-Based Computational Modeling in Cancer Biology,” *JCO Clinical Cancer Informatics*, (3), pp. 1–13.

- [54] Chimal-Eguía, J. C., Castillo-Montiel, E., and Paez-Hernández, R. T., 2020, “Properties of the Vascular Networks in Malignant Tumors,” *Entropy*, **22**(2), p. 166.
- [55] Fritz, M., Jha, P. K., Köppl, T., Oden, J. T., and Wohlmuth, B., 2021, “Analysis of a New Multispecies Tumor Growth Model Coupling 3D Phase-Fields with a 1D Vascular Network,” *Nonlinear Analysis: Real World Applications*, **61**, p. 103331.
- [56] Gautherie, M., 1982, “Temperature and Blood Flow Patterns in Breast Cancer during Natural Evolution and Following Radiotherapy,” *Prog Clin Biol Res*, **107**, pp. 21–64.
- [57] Said Camilleri, J., Farrugia, L., Curto, S., Rodrigues, D. B., Farina, L., Caruana Dingli, G., Bonello, J., Farhat, I., and Sammut, C. V., 2022, “Review of Thermal and Physiological Properties of Human Breast Tissue,” *Sensors*, **22**(10), p. 3894.
- [58] Schneck, D. J., 2014, “An Outline of Cardiovascular Structure and Function,” *Biomedical Engineering Fundamentals*, CRC Press, p. 14.
- [59] “Tissue Properties, Heat Capacity.”
- [60] “Tissue Properties, Thermal Conductivity.”
- [61] Gutierrez, C., 2024, “Clinical Validation of Patient-Specific Inverse Modeling with Surface Temperatures and Physiological and Geometrical Factors in Breast Cancer Detection.”
- [62] Mashekova, A., Zhao, Y., Ng, E. Y. K., Zarikas, V., Fok, S. C., and Mukhmetov, O., 2022, “Early Detection of the Breast Cancer Using Infrared Technology – A Comprehensive Review,” *Thermal Science and Engineering Progress*, **27**, p. 101142.
- [63] J. Gordon Betts, Kelly A. Young, James A. Wise, Eddie Johnson, Brandon Poe, Dean H. Kruse, Oksana Korol, Jody E. Johnson, Mark Womble, and Peter DeSaix, 2013, *Anatomy and Physiology*, OpenStax, Houston, Texas.
- [64] Incropera, F. P., DeWitt, D. P., Bergman, T. L., and Lavine, A. S., eds., 2007, *Fundamentals of Heat and Mass Transfer*, Wiley, Hoboken, NJ.
- [65] Kandlikar, S. G., ed., 2006, *Heat Transfer and Fluid Flow in Minichannels and Microchannels*, Elsevier, Amsterdam, Netherlands ; Boston.

[66] “Breast Cancer Statistics: How Common Is Breast Cancer?,” Breast Cancer Statistics | How Common Is Breast Cancer?